UNIVERSITY OF CALIFORNIA
SANTA CRUZ

EFFECTS OF SOLUBILIZING AGENTS ON THE PHOTOKINETICS OF RHODOPSIN

A dissertation submitted in partial satisfaction
of the requirement for the degree of

DOCTOR OF PHILOSOPHY

in

CHEMISTRY

by

Stephanie G. Pitch

December 2022

The Dissertation of Stephanie G. Pitch
is approved:

Professor David S. Kliger, Advisor

Professor Ólöf Einarsdóttir, Chair

Professor Seth Rubin

Peter Biehl
Vice Provost and Dean of Graduate Studies

TABLE OF CONTENTS

List of Figures

Abstract

EFFECTS OF SOLUBILIZING AGENTS ON THE PHOTOKINETICS OF RHODOPSIN

Stephanie G. Pitch

The native lipid environment is essential to the functional integrity of membrane proteins. Obtaining detailed information about the dynamics, mechanisms of action and structures of membrane proteins can be challenging, as traditional methods of solubilizing biological membranes can affect the preservation of surrounding lipid molecules. Novel solubilizing agents have been developed to maintain the stability of membrane proteins and improve the application of various biophysical techniques to study them. Unfortunately, in many cases, it is not clear if these solubilizing agents provide a truly natural environment or if they affect the functional properties of membrane proteins.

We address this question by comparing the photoactivation kinetics of rhodopsin, a G protein-coupled receptor (GPCR) in the disc membranes of rod cells, in native membrane suspensions, and in the solubilized state. Rhodopsin provides an ideal model system to investigate the functional integrity of a membrane protein because its activation mechanism is initiated with light, and the progression of the reaction intermediates can be monitored with absorption spectroscopy. The kinetics associated with rhodopsin intermediates are well documented at ambient temperature, so we can characterize any deviation to determine the effects due to solubilizing agents. Amphipathic copolymers, detergents, and membrane scaffold proteins were

investigated to evaluate the most suitable environment for studies of rhodopsin photokinetics.

Styrene maleic acid and diisobutylene maleic acid copolymers significantly slowed the reaction progress of rhodopsin, especially at late stages where significant conformational changes occur. While the highest styrene maleic acid/rhodopsin ratios yielded the most solubilized protein, the rhodopsin produced under these conditions could not reach the active (Meta II) state upon photoactivation and the changes to the protein were not reversible. In contrast, rhodopsin in lauryl maltose neopentyl glycol detergent micelles and membrane scaffold protein nanodiscs present native membrane-like intermediates without perturbing the activation sequence. The results presented in this dissertation may apply to many membrane-bound GPCR proteins.

Acknowledgments

This research would not have been possible without my Ph.D. advisor, Professor David Kliger, and I am thankful I had the opportunity to work in his lab. I appreciate his guidance and the time he dedicated to helping me improve as a scientist. Many thanks to my committee members, Professors Ólöf Einarsdóttir and Seth Rubin, who provided thoughtful suggestions and advice on project management.

To our group researchers, Dr. Eefei Chen and Dr. Istvan Szundi, thank you for ensuring experiments ran smoothly and sharing your expertise in data analysis. The project would not be where it is today without the contributions of Dr. Jim Lewis. I appreciate his insight and advice immensely. I would also like to mention other members of the Kliger Lab, especially Dr. Chie Funatogawa, Dr. Pamela Schleissner, Vivian, and Conrad. It was great working with all of you.

The results presented in this dissertation would not be possible without our collaborators. Big thanks to Professor David Farrens and Weekie Yao (Oregon Health and Science University), who provided the SMA(3:1) copolymer, along with Professor Barry Bruce, Professor Brian Long, and Cameron Workman (University of Tennessee, Knoxville), who provided the series of functionalized SMA(1.2:1) copolymers.

A special thanks to Dr. Caitlin Binder for asking me to build websites when the organic chemistry teaching lab switched to remote learning. It was a big challenge, but we received a lot of positive feedback from students, which was very rewarding.

I started this journey thanks to my undergraduate advisor, Professor Kjirsten Wayman. I admire so much about her and her research on western *Trillium*.

I could not have completed this program without encouragement from my family and loved ones, especially my mom, dad, grandma and grandpa, Aunt Laura, Uncle Geoff, Scott, Lily, and Orion. Thanks for always cheering me on.

To my husband, Gregory, thank you for everything- from helping me navigate challenging projects to encouraging me to surf Pleasure Point instead of 38th when the waves were good. I am so grateful to have you in my life. To our pups, Mocha and Earl, your playful energy is contagious, and your goofy personalities always make me laugh. And to our daughter, Piper, being your mom fills my heart with joy. I love you more than words can describe.

For

Gregory Matthew & Piper Grace

CHAPTER 1 Rhodopsin

1.1 Phototransduction

Rod and cone photoreceptor cells in the retina capture light and convert it into electrical signals in a process known as phototransduction. The human retina contains 120 million rod cells that operate under dim lighting conditions, and 6 million cone cells that function under bright lighting conditions.[1] The rods and cone cells consist of five parts: the outer segment (OS), connecting cilium (CC), inner segment (IS), nuclear region, and synaptic region (Figure 1.1.1). The rod outer segment (ROS) has been the focus of numerous biochemical and physiological studies due to their abundance, ease of isolation, and importance in retinal diseases. The ROS is a cylindrical structure that encloses an ordered stack of over 1000-2000 closely spaced discs. The G-protein coupled receptor (GPCR) rhodopsin is the major protein component of the bilayered disc membrane and occupies approximately half of the membrane area, while phospholipids (85-90 mol% of total lipids) and cholesterol (8-10 mol% of total lipids) mainly fill the remaining space.[2]

There are approximately 65-70 phospholipids per rhodopsin molecule.[3,4] The average disc membrane is composed of 44% phosphatidylcholine, 41% phosphatidylethanolamine, 13% phosphatidylserine, and 2% phosphatidylinositol. Phospholipids that surround rhodopsin not only serve as a structural support, but also influence the protein's function through direct interactions with the lipid headgroups and acyl chains. ROS disc membranes are exceptionally rich in docosahexaenoic acid (~80 mol% of total polyunsaturated fatty acids), which is known to significantly

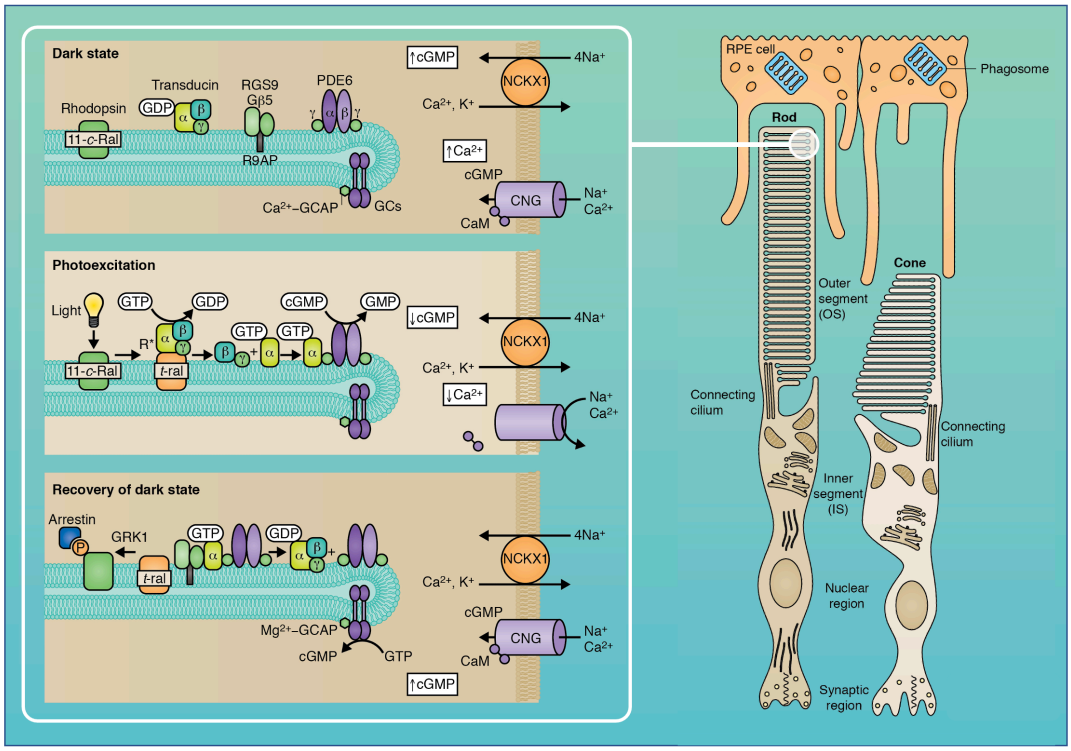

Figure 1.1.1 Photoreceptors (right) and activation of rhodopsin in rod outer segment disc membrane (left). Light isomerizes the chromophore 11-*cis*-retinal (11-c-Ral) to all-*trans*-retinal (t-ral), which leads to conformational changes in the protein and formation of the active state of rhodopsin, metarhodopsin II (R*). The activated form of rhodopsin initiates a biochemical cascade involving G-protein transducin. Figure from doi.org/10.1242/jcs.175687.

contribute to visual function in rats.[5] The effect of the lipid bilayer on the activation of rhodopsin has been studied in great detail by the laboratories of Litman and Mitchell, Brown, and Gawrisch.[6–10]

Phototransduction in rod cells begins when a single photon isomerizes the 11-*cis*-retinal chromophore of rhodopsin to its all-*trans* isomer (Figure 1.1.1). Isomerization occurs within 200 femtoseconds and has a quantum yield of 0.65±0.01 between 450 and 500 nm.[11,12] After isomerization, rhodopsin goes through a series of

intermediates that first involve structural changes local to the chromophore but eventually result in global conformational changes that enable binding active receptor to the G protein, transducin. The subsequent activation of transducin initiates an enzyme cascade, which closes sodium channels in the rod cells. The resulting hyperpolarization of the rod cells inhibits the release of the neurotransmitter glutamate at the photoreceptor synapse. This causes a change in electrical current through the cells and thus detection of light. Mutations within most of the phototransduction proteins are associated with retinal diseases.

1.2 Structure and Activation of Rhodopsin

Rhodopsin is comprised of the 40-kDa apoprotein opsin and its chromophore, 11-*cis*-retinal (Figure 1.2.1). Bovine opsin has 348 amino acids. It contains seven transmembrane α-helices (H1-H7), an extracellular/intradiscal N-terminal region, and a cytoplasmic/intracellular C-terminal region. A short cytoplasmic helix, H8, follows H7, and the former is tethered to the membrane by palmitoylated Cys residues. There are three cytoplasmic loops (C1-C3) and three extracellular loops (E1-E3) that connect the transmembrane helices. The transmembrane region contains ~65% of the amino acids, while the remaining 35% are distributed fairly evenly between the cytoplasmic and extracellular compartments of the cell.

The chromophore forms a protonated Schiff base (PSB) linkage to Lys^{296} within the transmembrane region of H7. A highly conserved residue among vertebrate visual pigments, Glu^{113}, serves as a counterion for the PSB and is a key constraint for the dark

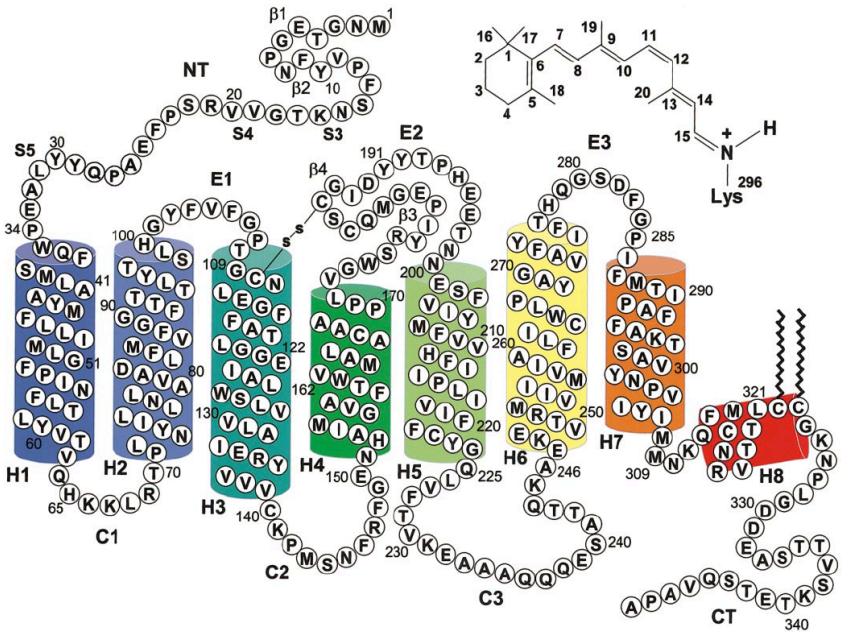

Figure 1.2.1 Secondary structure of bovine rhodopsin. The transmembrane α-helical segments H1-H7 and amphipathic helix H8 are displayed as colored cylinders. The structure of the 11-*cis*-retinylidene chromophore bound to Lys^{296} via a protonated Schiff base is displayed in the top right. Figure from doi.org/10.1152/physrev.2001.81.4.1659.

state of the receptor. The counterion stabilizes the PSB by increasing the K_a and thus preventing spontaneous hydrolysis. The negative charge on Glu^{113} also delocalizes the positive charge of the PSB into the conjugated system of 11-*cis*-retinal. As a result, there is a bathochromic shift in the maximum absorption that makes visual pigments more sensitive to longer wavelengths. This sensitivity to longer wavelengths is essential for vision since UV light is filtered out by the front of the eye in most animals. The rigid-body rotation of helix H6 away from the rest of the helix bundle is a key event during the activation of rhodopsin (Figure 1.2.2). The disruption of the salt bridge between the cationic PSB and anionic counterion triggers the TM6 motion that occurs

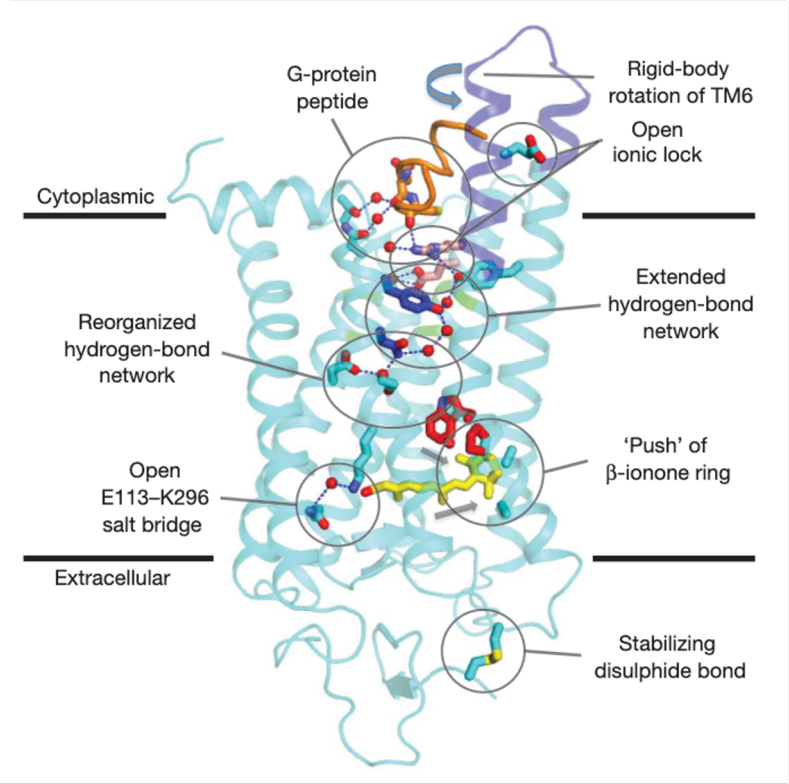

Figure 1.2.2 Activation of rhodopsin and changes that result in G protein binding. Predominant conformational changes in H5 and H6 in blue. The side chains of the NPXXY motif (blue) extend the hydrogen-bond network through the hydrophobic barrier (green). Side chains of the E(D)RY motif, part of the ionic lock and the G protein-binding site, are in pink. Figure from doi.org/10.1038/nature09795

upon isomerization. This conformational change is amplified by a characteristic bend in the retinal pocket caused by Pro^{267}, which is one of the most conserved residues among GPCRs and part of the CWXP motif. This motif also contains Trp^{265}, a residue that is tightly packed against the retinal in the dark state of rhodopsin and has been shown to be important for activation through mutagenesis studies.[13]

Other highly conserved domains among GPCRs, including E(D)RY in H3 and NPXXY in H7, are important for rhodopsin to transform from the inactive state to the

G protein–coupled conformation. The chromophore pocket of ground-state rhodopsin is connected with Asn^{302} of the NPXXY motif via a water-mediated hydrogen-bond network.[14] A hydrophobic barrier made up of residues Leu^{76}, Leu^{79}, Leu^{128}, Leu^{131}, and Met^{257} separates the NPXXY motif from the E(D)RY motif. The rotation of H6 opens up this barrier, allowing Tyr^{223} and Tyr^{306} of the NPXXY motif to move towards the protein interior. The phenolic side chains extend the hydrogen-bond network up to the E(D)RY motif, which disrupts ionic interactions between Glu^{134}/Arg^{135} and Glu^{247} and allows G protein interaction.

1.3 Reaction Mechanism and Photointermediates

During the conversion from an inactive to active state, rhodopsin goes through a series of photointermediates whose absorption maxima are distinct from each other. Early studies on the reaction mechanism of rhodopsin involved low-temperature trapping methods to stabilize the intermediates involved in the activation process. The ability to trap unstable intermediates at low temperature allowed researchers to elucidate the driving forces responsible for the reaction mechanism before structural methods with time resolution were available.[15] The emergence of fast laser excitation sources made it possible to probe intermediates that are detected at physiologically relevant temperatures. The Kliger laboratory recently described the kinetics of the activation mechanism of rhodopsin as a double-square model (Figure 1.3.1).[16] The double-square model reflects how the activation mechanism varies depending on temperature and pH conditions.

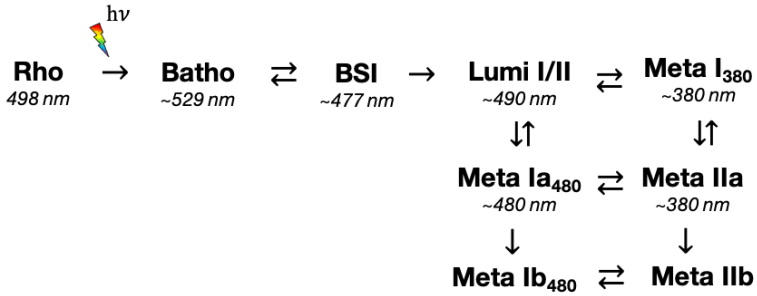

Figure 1.3.1 Double-square model of the rhodopsin activation mechanism.

The first intermediate, bathorhodopsin (Batho, λ_{max} = ~529 nm), appears within a picosecond. Batho contains the all-*trans* form of the chromophore, and torsional strain on the chromophore allows Batho to store a large fraction of the original photon energy. As the twisted chromophore relaxes, Batho enters an equilibrium with a blue-shifted intermediate (BSI, λ_{max} = ~477 nm). BSI is not observed during low-temperature trapping experiments since there is a substantial back-reaction from BSI to Batho. At low temperatures, the equilibrium constant shifts such that BSI never accumulates. Studies involving analogs of retinal have shown that the formation rate of BSI depends on the structural details of the chromophore, while the decay rate is relatively independent of the chromophore.[17] Therefore, the rate-limiting step in BSI decay is thought to involve protein relaxation.

After a few hundred nanoseconds, the Batho to BSI equilibrium decays into an equilibrated mixture of lumirhodopsin I and II (Lumi I/II, λ_{max} = ~490 nm) in tens of microseconds. While the submicrosecond kinetics of rhodopsin after photoexcitation are unaffected by the surrounding environment, the decays following the Lumi equilibrium are dramatically increased in detergent solubilized systems.[18] This finding

is consistent with the idea that late conformational changes of the protein that lead to the active state are sensitive to the lipid environment. The Lumi I/II equilibrium then branches to form two different metarhodopsin intermediates. One absorbs at 380 nm (Meta I_{380}) while the other absorbs at 480 nm (Meta Ia_{480}), and these transitions occur on a similar time scale. Both intermediates convert to the active state, metarhodopsin II (Meta IIa, λ_{max} = ~380 nm), within tens of milliseconds via a reversible step.

The double-square model was derived from a study on the photoactivation kinetics of rhodopsin at 15°C and alkaline pH, which showed that the kinetic scheme was more complex than originally thought. To fit the data that was obtained at a range of pH values, two isospectral Meta I_{480} states were introduced (hence the *a* and *b* denotations in their names). The first, Meta Ia_{480}, is formed from Lumi I/II via a reversible step, and then converts to the second, Meta Ib_{480}, via an irreversible step. Both states form their deprotonated counterparts, Meta IIa and Meta IIb, by a reversible step.

1.4 Aims of the Study

The goal of this study is to test whether rhodopsin solubilized into lipid nanoparticles preserves the functional properties it has in its native membrane. Since ROS disc membrane contains rhodopsin almost exclusively (~90%), the amount of protein solubilized can be quantified by measuring the absorbance of the sample and comparing that to the original amount of protein in the native membrane. Additionally, rhodopsin provides an ideal model system to analyze the functional integrity of a

solubilized protein. The activation mechanism is initiated with light, so absorption spectroscopy can monitor the progression of the reaction intermediates. Since the molecular intermediates involved in rhodopsin's activation mechanism absorb different wavelengths of light, their concentrations can be monitored spectroscopically, which allows us to judge the protein's ability to function in different environments.

The research discussed here was performed on bovine retinas, which yield about 0.5-1 mg rhodopsin per retina.[19] Bovine and human rhodopsin have similar amino acid sequences, with only 23 positions having different residues (93.4% sequence identity).[20] Both follow the same kinetic scheme, the double-square model, but there are differences in the favored reaction pathway and thus the intermediates that accumulate.[21] Nonetheless, research conducted on bovine rhodopsin may be relevant to human visual perception or apply to other membrane-bound GPCR proteins. The focus of this study was on reaction steps that follow the formation of the Lumi intermediate and lead to the active-state Meta II, since these steps are known to be more sensitive to the membrane environment. We first want to understand the effect that solubilizing agents have on these later intermediates to study mutations within rhodopsin involved with retinal diseases.

1.5 References

(1) Molday, R. S.; Moritz, O. L. Photoreceptors at a Glance. *J. Cell Sci.* 2015, *128* (22), 4039. https://doi.org/10.1242/jcs.175687.

(2) Palczewski, K. G Protein–Coupled Receptor Rhodopsin. *Biochemistry* 2006, *75* (1), 743–767. https://doi.org/10.1146/annurev.biochem.75.103004.142743.

(3) Aveldaño, M. I. Phospholipid Solubilization during Detergent Extraction of Rhodopsin from Photoreceptor Disk Membranes. *Arch Biochem Biophys* 1995, *324* (2), 331–343. https://doi.org/10.1006/abbi.1995.0046.

(4) Jastrzebska, B.; Debinski, A.; Filipek, S.; Palczewski, K. Role of Membrane Integrity on G Protein-Coupled Receptors: Rhodopsin Stability and Function. *Prog. Lipid Res.* 2011, *50* (3), 267–277. https://doi.org/10.1016/j.plipres.2011.03.002.

(5) Mitchell, D. C.; Niu, S.-L.; Litman, B. J. Enhancement of G Protein-Coupled Signaling by DHA Phospholipids. *Lipids* 2003, *38* (4), 437–443. https://doi.org/10.1007/s11745-003-1081-1.

(6) Litman, B. J.; Mitchell, D. C. A Role for Phospholipid Polyunsaturation in Modulating Membrane Protein Function. *Lipids* 1996, *31* (1Part2), S193–S197. https://doi.org/10.1007/bf02637075.

(7) Niu, S.-L.; Mitchell, D. C.; Lim, S.-Y.; Wen, Z.-M.; Kim, H.-Y.; Salem, N.; Litman, B. J. Reduced G Protein-Coupled Signaling Efficiency in Retinal Rod Outer Segments in Response to n-3 Fatty Acid Deficiency*. *J Biol Chem* 2004, *279* (30), 31098–31104. https://doi.org/10.1074/jbc.m404376200.

(8) Brown, M. F. Influence of Nonlamellar-Forming Lipids on Rhodopsin. *Curr Top Membr* 1997, *44*, 285–356. https://doi.org/10.1016/s0070-2161(08)60212-9.

(9) Brown, M. F. Modulation of Rhodopsin Function by Properties of the Membrane Bilayer. *Chem Phys Lipids* 1994, *73* (1–2), 159–180. https://doi.org/10.1016/0009-3084(94)90180-5.

(10) Gawrisch, K.; Soubias, O. Structure and Dynamics of Polyunsaturated Hydrocarbon Chains in Lipid Bilayers—Significance for GPCR Function. *Chem Phys Lipids* 2008, *153* (1), 64–75. https://doi.org/10.1016/j.chemphyslip.2008.02.016.

(11) Peteanu, L. A.; Schoenlein, R. W.; Wang, Q.; Mathies, R. A.; Shank, C. V. The First Step in Vision Occurs in Femtoseconds: Complete Blue and Red Spectral Studies. *Proc National Acad Sci* 1993, *90* (24), 11762–11766. https://doi.org/10.1073/pnas.90.24.11762.

(12) Kim, J. E.; Tauber, M. J.; Mathies, R. A. Wavelength Dependent Cis-Trans Isomerization in Vision †. *Biochemistry-us* 2001, *40* (46), 13774–13778. https://doi.org/10.1021/bi0116137.

(13) Ridge, K. D.; Bhattacharya, S.; Nakayama, T. A.; Khorana, H. G. Light-Stable Rhodopsin. II. An Opsin Mutant (TRP-265—-Phe) and a Retinal Analog with a

Nonisomerizable 11-Cis Configuration Form a Photostable Chromophore. *J Biol Chem* 1992, *267* (10), 6770–6775. https://doi.org/10.1016/s0021-9258(19)50492-6.

(14) Standfuss, J.; Edwards, P. C.; D'Antona, A.; Fransen, M.; Xie, G.; Oprian, D. D.; Schertler, G. F. X. The Structural Basis of Agonist-Induced Activation in Constitutively Active Rhodopsin. *Nature* 2011, *471* (7340), 656–660. https://doi.org/10.1038/nature09795.

(15) Lewis, J. W.; Kliger, D. S. Photointermediates of Visual Pigments. *J. Bioenerg. Biomembr.* 1992, *24* (2), 201–210. https://doi.org/10.1007/bf00762678.

(16) Szundi, I.; Funatogawa, C.; Kliger, D. S. Complexity of Bovine Rhodopsin Activation Revealed at Low Temperature and Alkaline PH. *Biochemistry* 2016, *55* (36), 5095–5105. https://doi.org/10.1021/acs.biochem.6b00687.

(17) C. E. Randall; J. W. Lewis; S. J. Hug,; S. C. Bjórling,; I. Eisner-Shanas,; N. Friedman; M. Ottolenghi,; M. Sheves; D. S. Kliger. A New Photolysis Intermediate in Artificial and Native Visual Pigments. *J. Am. Chem. Soc.* 1991, *113* (9), 3473–3485. https://doi.org/10.1021/ja00009a037.

(18) Epps, J.; Lewis, J. W.; Szundi, I.; Kliger, D. S. Lumi I → Lumi II: The Last Detergent Independent Process in Rhodopsin Photoexcitation. *Photochem. Photobiol.* 2006, *82* (6), 1436–1441. https://doi.org/10.1562/2006-02-01-ra-792.

(19) Filipek, S.; Stenkamp, R. E.; Teller, D. C.; Palczewski, K. G Protein-Coupled Receptor Rhodopsin: A Prospectus. *Annu Rev Physiol* 2003, *65* (1), 851–879. https://doi.org/10.1146/annurev.physiol.65.092101.142611.

(20) Kazmin, R.; Rose, A.; Szczepek, M.; Elgeti, M.; Ritter, E.; Piechnick, R.; Hofmann, K. P.; Scheerer, P.; Hildebrand, P. W.; Bartl, F. J. The Activation Pathway of Human Rhodopsin in Comparison to Bovine Rhodopsin. *J Biol Chem* 2015, *290* (33), 20117–20127. https://doi.org/10.1074/jbc.m115.652172.

(21) Funatogawa, C.; Szundi, I.; Kliger, D. S. A Comparison between the Photoactivation Kinetics of Human and Bovine Rhodopsins. *Biochemistry* 2016, *55* (50), 7005–7013. https://doi.org/10.1021/acs.biochem.6b00953.

CHAPTER 2 Experimental Methods and Spectral Analysis

2.1 Isolating Rhodopsin from ROS Disc Membrane

All rhodopsin samples were prepared from bovine retinas (Wanda Lawson, Omaha, NE).[1] The rhodopsin samples required separation and purification of the rod outer segments (ROS) from the retina. Sample preparation and the experiments that followed were carried out under red light. Centrifuge spins were done at 4°C in a Sorvall SS-34 fixed angle rotor, except where otherwise noted. The solutions required for this step include TBS buffer [10 mM tris(hydroxymethyl)aminomethane, 60 mM KCl, 30 mM NaCl, 2 mM MgCl, and 0.1 mM EDTA, with ≈1 mM dithiothreitol (disulfide reducing agent) and 0.01 μL aprotinin/mL solution (trypsin inhibitor), adjusted to pH 7 at 4°C], and 33% (w/v) or 43% (w/v) sucrose in TBS buffer. Both sucrose concentrations were determined with the use of a Milton Roy Abbe benchtop refractometer. All other reagents were purchased from Sigma Aldrich or Fisher Scientific, unless otherwise specified.

Dark-adapted retinas were shipped frozen in aluminum foil-covered jars with 43% sucrose at a concentration of 50 retinas per 25 mL TBS buffer. The jars were shaken vigorously for 60 seconds, and then the contents were transferred into two 35 mL centrifuge tubes. The solutions were centrifuged at 3,000 x g for 5 minutes. The supernatant was transferred into four centrifuge tubes, and the pellets were rinsed gently with TBS buffer before being discarded. TBS was added to fill the remaining volume of the centrifuge tubes. The solutions were mixed well before they were centrifuged at 27,000 x g for 15 minutes. The resulting supernatant was carefully

removed, and the pellets were resuspended with ~25 mL of 33% sucrose. The ROS suspension was divided equally into two centrifuge tubes and overlayed with TBS buffer while avoiding disrupting the bottom layer. The samples were centrifuged at 16,000 x g for 4 hours in a Sorvall HB-4 swinging bucket rotor. The ROS layer between the sucrose solution and the TBS was collected with a flat-tipped needle while being careful to leave the heavier sucrose layer behind. The ROS layers collected were combined into one centrifuge tube and mixed thoroughly.

The concentration of rhodopsin in the solution was determined using a Jasco V-750 UV-Vis Spectrophotometer. A small aliquot was diluted in 3% (v/v) Ammonyx LO in TBS. An absorption spectrum of the dark-state rhodopsin was measured from 250-700 nm at room temperature. The sample was then irradiated for 30 s using a tungsten-halogen lamp (150 W) placed six inches away from the sample holder with a yellow filter in front. Shortly after irradiating the sample, a second absorption spectrum was measured. The change in absorbance at 500 nm (ε = 40,600 $M^{-1}cm^{-1}$) before and after irradiation, multiplied by the dilution factor, is equal to the concentration of rhodopsin in mg/mL. ROS samples were typically between 1 to 2 mg/mL. Additionally, the 280 nm/500 nm absorbance ratio for the dark-state rhodopsin measures the purity of the ROS preparation. This method typically results in a ratio between 2 and 3. The sample was evenly distributed into 8-mL screw cap vials, wrapped in foil, and stored at -75°C.

A hypotonic wash was performed to isolate the disc membrane from the rod outer segment. The ROS samples from the preparation above were thawed for 20

minutes and transferred to a centrifuge tube. The screw-cap vials were rinsed with TBS buffer, and then the suspension was centrifuged for 20 minutes at 34,000 x g. Next, the supernatant was removed, and the pellet was resuspended in 20 mL of EDTA solution (1 mM EDTA, adjusted to pH 7.0 at 4°C). The sample was centrifuged for one hour at 34,000 x g. The previous resuspension/spin step was repeated. After discarding the supernatant from the second EDTA wash, the pellet was resuspended in 15 mL of TBS buffer and centrifuged at 34,000 x g for 20 minutes. The resulting pellets were resuspended in TBS to a final concentration of 1-1.5 mg rhodopsin/mL. The hypotonically washed ROS membrane suspension was divided into 1-mL aliquots, wrapped in foil, and stored at -75°C. Before use, samples were thawed in the dark and then centrifuged at 17,000 x g for 20 minutes to carry out a buffer exchange.

2.2 Static Photobleaching Measurements

Rhodopsin samples were characterized by their optical absorption spectra measured using a Jasco V-750 UV-Vis Spectrophotometer in the 250-700 nm wavelength range at room temperature. An absorption spectrum was measured after adding a solubilizing agent, such as styrene-maleic acid copolymer, to the membrane suspension (Figure 2.2.1). Next, the sample was centrifuged to isolate the soluble fraction. An absorption spectrum of the soluble fraction was collected to determine the solubilization efficiency. Then, an additional absorption spectrum was recorded after irradiating the samples for 30 s to characterize the functional properties of the solubilized rhodopsin.

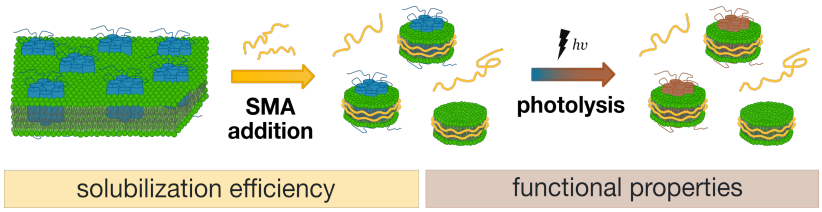

Figure 2.2.1 Schematic diagram of static photobleaching experiments with solubilizing agents like styrene maleic acid (SMA) copolymer and rhodopsin.

2.3 Collecting Time-Resolved Absorption Spectra

The activation kinetics of the rhodopsin samples were investigated using time-resolved optical absorption (TROA) spectroscopy. The reaction was initiated by a ~7 ns pulse of 477 nm light (80 μJ/mm^2) generated by a Spectra-Physics PDL-2 dye laser containing Coumarin 480 in methanol, which is pumped by the third harmonic (355 nm) of a Quanta-Ray DCR-2 Q-switched Nd:YAG laser (Figure 2.3.1a).[2,3] Absorption spectra were recorded before and after laser photolysis in the 330-630 nm wavelength range at selected logarithmically spaced delay times using a microscale apparatus.

A multiwavelength time-resolved absorption apparatus was used to obtain spectra of the reaction products (or mixture) formed by laser photolysis (Figure 2.3.1b).[4,5] The laser beam enters the sample at a 90° angle to the probe beam, produced by an EG&G FXQ-856 Xenon short-arc flash lamp. A pulse of white light from the flash lamp was used to measure the absorbance changes. Beam flags were placed in front of both light sources to control which one entered the sample for the different

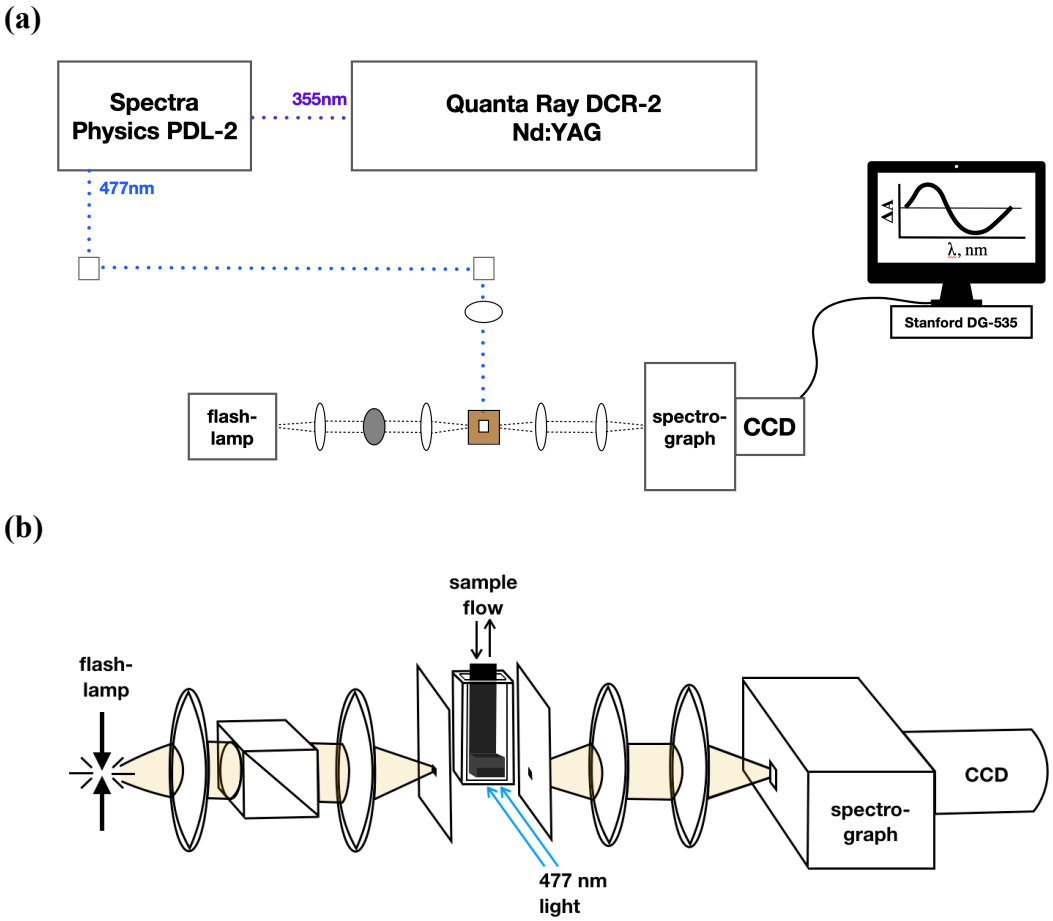

Figure 2.3.1 (a) Experimental set-up for measuring time-resolved optical absorption difference spectra of rhodopsin samples. **(b)** Close-up of the microscale apparatus. Rhodopsin samples are flowed into the optical path contained under the cuvette insert. Absorbance changes are probed with light from the flash lamp, which are focused onto the sample with two spherical lenses. Once the sample is photolyzed with a pulse of 477-nm actinic light, two spherical lenses collimate and re-focus the transmitted beam into the spectrograph.

measurements. The incident light was focused onto the sample, and the transmitted light was refocused onto a 250 μm slit of a Jarrell-Ash Monospec 25 0.25-m spectrograph equipped with a 150 groove per mm grating. The spectrograph disperses the light across the channels of an Andor DH-520 intensified charge-coupled device

(CCD). A Stanford Research Systems DG535 digital delay generator synchronized the gate pulses applied to the laser, flash lamp, and OMA detector.

An insert was placed into a 4 mm x 4 mm cuvette (Starna Cells Inc., Atascadero, CA) to form a 2 μL sample chamber at the bottom, with a height of 1 mm and an actinic pathlength of 0.5 mm, contained between the cuvette walls. A l/2 cc glass syringe driven by a linear stepper motor was used to pump a fresh sample after each photolysis pulse.[6] At the same time, a channel on the insert allowed photolyzed material that is no longer usable to leave and collect outside of the sample path in the cuvette. The temperature of the sample was regulated with a copper insert connected to a thermostated water bath.

2.4 Analysis of Static Absorption Spectra

The static spectra are analyzed using MATLAB (MathWorks). Each recorded spectrum is corrected for light scattering contributions and absorbance due to the solubilizing agents (for example, λ_{max} = 260 nm for styrene-maleic acid copolymers). The light scattering function for molecules and small particles is $\sim\lambda^{-4}$, and the approximation applicable to big particles is $\sim\lambda^{-2}$. Sometimes, a combination of both functions was required to produce the corrected spectra. The spectra recorded prior to photobleaching were normalized to 1 A.U. at 500 nm. The same normalization factors were used to adjust the amplitudes of the spectra obtained after photobleaching. This allowed us to quantitatively assess the spectral forms of rhodopsin photoproducts in the irradiated samples.

2.5 Analysis of Time-Resolved Optical Absorption Spectra

The spectral analysis for the time-resolved optical absorption data presented below was carried out using scripts written in MATLAB (MathWorks).

The analysis is based on the assumption that all reactions involved in the photolysis are of first order and can be described by a set of first-order differential equations. The concentration time dependence of such a reaction set is described by a sum of exponential functions. The time dependent absorption difference spectra (post- minus pre-photolysis) enclosed in the experimental data matrix thus can also be fitted globally to a sum of exponentials as displayed in Equation 2.1,

$$\Delta\mathbf{a}(\lambda,t) = \Sigma\, b_i(\lambda)\exp(-r_i \times t) + b_0(\lambda) \qquad (2.1)$$

where the r_i's are the apparent rate constants, and $b_i(\lambda)$ and $b_0(\lambda)$ are the amplitudes of the time-dependent and time-independent difference spectra, respectively, which are referred to as b-spectra.[7,8]

Based on the assumption that all observed reactions are first order, the experimental difference spectra (post- minus pre-photolysis) recorded at various wavelengths and delay times [$\Delta\mathbf{A}(\lambda,t)$] are analyzed with singular value decomposition (SVD), followed by global exponential fitting. First, SVD is utilized to reduce noise in the spectral data and estimate the number of spectrally distinct intermediates required to yield the observed spectral changes at the measurement times. The spectral and the temporal information in the data matrix are separated using Equation 2.2,

$$\Delta\mathbf{A} = \mathbf{U} \times \mathbf{S} \times \mathbf{V}^T \qquad (2.2)$$

where **U** is the matrix of orthonormal spectral vectors, **V** is the matrix of orthonormal

temporal vectors, and **S** is a diagonal matrix of the significance values, which are the contributions of the individual **U** and **V** vector-pairs to the data matrix.

Only the significant time-dependent vectors, **V**(n), are globally fitted to sums of exponentials yielding the apparent rates. The b-spectra are calculated by combining the results of the exponential fit with the significant spectral vectors, **U**(n).[9] The quality of the fit is judged by a plot of the residuals, which is the difference between the experimental data and the reproduced data.

2.5.A Deconvolution of Sequential Intermediate Spectra

The b-spectra from the exponential fit are difficult to deconvolute into spectra of the molecular intermediate states. Spectra of a straight sequential scheme are better suited for this purpose. Thus, the b-spectra arranged in the **B**(λ,n) matrix were converted into the spectra of the sequential intermediates enclosed in the **In**(λ,n) matrix, as shown in Equation 2.3,

$$\mathbf{In}(\lambda,n) = \mathbf{B}(\lambda,n) \times \mathbf{W}^{-1} \tag{2.3}$$

where **W** is the eigenvector matrix of the kinetic matrix constructed for the straight sequential scheme in which the apparent rates, r_i, are assigned to the reaction rates between the intermediates.

In a straight sequential scheme without back reaction, the apparent rates are equal to the microscopic rate constants, and it is the only scheme in which the intermediate spectra can be calculated from the experimental data without further assumptions. The intermediate spectra are interpreted as sums of the spectral forms and are mathematically defined in Equation 2.4,

$$\mathbf{In}(\lambda,n) = \mathbf{E}(\lambda,m) \times \mathbf{Q}(m,n) \quad (2.4)$$

where $\mathbf{E}(\lambda,m)$ is the matrix of the m spectral forms and $\mathbf{Q}(m,n)$ is the composition matrix of the n sequential intermediates.

The Rho, Lumi, $Meta_{480}$, $Meta_{460}$, and $Meta_{380}$ spectral forms (Figure 2.5.A.1) used to determine the composition of the intermediate spectra were obtained the following way. The Rho, $Meta_{480}$, and $Meta_{380}$ spectral forms are from the static spectra (Section 2.2). The Lumi spectral form is the experimental spectrum of the first sequential intermediate. Lastly, the $Meta_{460}$ spectral form is a blue-shifted variant of the $Meta_{480}$ spectral form. $Meta_{460}$ is a characteristic component of the spectral forms that are detected on the seconds-to-minutes timescale during the deactivation of rhodopsin.[10,11] A fraction of the Rho spectrum was added to the intermediate difference

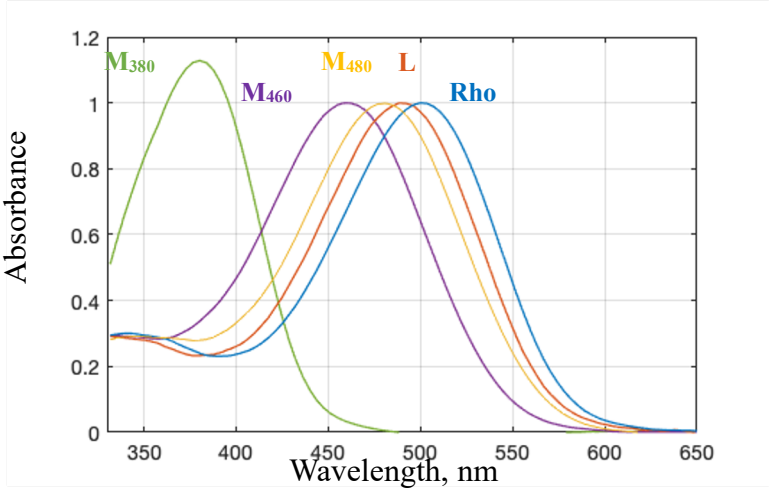

Figure 2.5.A.1 Model spectra of rhodopsin (Rho), Lumi (L), $Meta_{480}$ (M_{480}), $Meta_{460}$ (M_{460}), and $Meta_{380}$ (M_{380}) used to determine the spectral composition of the intermediate spectra of the sequential scheme.

spectra to obtain the absolute spectra. In retinal proteins, the spectra of the intermediate states will have the same distribution on the energy scale. If too little of the Rho spectrum is added back to an intermediate spectrum, the shape will be narrow or have negative absorbance. When enough is added back, the spectrum will match the shape of others and have no negative absorbance.

The other spectral forms were used to determine the composition of each absolute spectrum, expressed as fraction numbers equal to one for each intermediate of the straight sequential scheme. These values are then used to construct the composition matrix, $\mathbf{Q}(m,n)$. The time evolution of the m spectral forms, $\mathbf{C_m}(n,t)$, can be calculated without knowing the reaction mechanism and is obtained using Equation 2.5,

$$\mathbf{C_m}(n,t) = \mathbf{Q}(m,n) \times \mathbf{C_{in}}(n,t) \tag{2.5}$$

where $\mathbf{C_{in}}(n,t)$ is the matrix of the time-dependent concentrations of the n sequential intermediates calculated using the kinetic matrix constructed for the straight sequential scheme.

A valid scheme must be able to reproduce the apparent rates and the experimental b-spectra from the spectra of the proposed intermediates. Often, the straight sequential scheme does not yield acceptable intermediate spectra, and reaction schemes with more steps are required. Nonetheless, the experimental b-spectra calculated from the straight sequential scheme provide key information to propose a kinetic mechanism, as their shapes show the decay and formation of molecular intermediate states. A fitting procedure designed to reproduce the experimental b-spectra and apparent rates is used to validate the proposed mechanism.

2.6 References

(1) Thorgeirsson, T. E.; Lewis, J. W.; Wallace-Williams, S. E.; Kliger, D. S. Photolysis of Rhodopsin Results in Deprotonation of Its Retinal Schiff's Base Prior to Formation of Metarhodopsin II. *Photochem. Photobiol.* 1992, *56* (6), 1135–1144. https://doi.org/10.1111/j.1751-1097.1992.tb09738.x.

(2) Lewis, J. W.; Yee, G. G.; Kliger, D. S. Implementation of an Optical Multichannel Analyzer Controller for Nanosecond Flash Photolysis Measurements. *Rev Sci Instrum* 1987, *58* (6), 939–944. https://doi.org/10.1063/1.1139579.

(3) Thorgeirsson, T. E.; Lewis, J. W.; Wallace-Williams, S. E.; Kliger, D. S. Effects of Temperature on Rhodopsin Photointermediates from Lumirhodopsin to Metarhodopsin II. *Biochemistry* 1993, *32* (50), 13861–13872. https://doi.org/10.1021/bi00213a015.

(4) Lewis, J. W.; Warner, J.; Einterz, C. M.; Kliger, D. S. Noise Reduction in Laser Photolysis Studies of Photolabile Samples Using an Optical Multichannel Analyzer. *Rev. Sci. Instrum.* 1987, *58* (6), 945–949. https://doi.org/10.1063/1.1139580.

(5) Lewis, J. W.; Kliger, D. S. Absorption Spectroscopy in Studies of Visual Pigments: Spectral and Kinetic Characterization of Intermediates. *Methods Enzymol.* 2000, *315*, 164–178. https://doi.org/10.1016/s0076-6879(00)15842-2.

(6) Lewis, J. W.; Kliger, D. S. Microliter Flow Cell for Measurement of Irreversible Optical Absorbance Transients. *Rev. Sci. Instrum.* 1993, *64* (10), 2828–2833. https://doi.org/10.1063/1.1144369.

(7) Hug, S. J.; Lewis, J. W.; Einterz, C. M.; Thorgeirsson, T. E.; Kliger, D. S. Nanosecond Photolysis of Rhodopsin: Evidence for a New Blue-Shifted Intermediate. *Biochemistry* 1990, *29* (6), 1475–1485. https://doi.org/10.1021/bi00458a019.

(8) Szundi, I.; Lewis, J. W.; Kliger, D. S. Deriving Reaction Mechanisms from Kinetic Spectroscopy. Application to Late Rhodopsin Intermediates. *Biophys. J.* 1997, *73* (2), 688–702. https://doi.org/10.1016/s0006-3495(97)78103-7.

(9) Henry, E. R.; Hofrichter, J. Singular Value Decomposition: Application to Analysis of Experimental Data. *Methods Enzymol.* 1992, *210*, 129–192. https://doi.org/doi: 10.1016/0076-6879(92)10010-B.

(10) Szundi, I.; Lewis, J. W.; Kuijk, F. J. G. M. van; Kliger, D. S. Effect of NADPH on Formation and Decay of Human Metarhodopsin III at Physiological Temperatures. *Vision Res* 2000, *40* (22), 3039–3048. https://doi.org/10.1016/s0042-6989(00)00148-6.

(11) Bartl, F. J.; Vogel, R. Structural and Functional Properties of Metarhodopsin III: Recent Spectroscopic Studies on Deactivation Pathways of Rhodopsin. *Phys Chem Chem Phys* 2007, *9* (14), 1648–1658. https://doi.org/10.1039/b616365c.

CHAPTER 3 Rhodopsin Solubilized by Styrene-Maleic Acid Copolymer

3.1 Differences from the Styrene Maleic Acid/Rhodopsin Molar Ratio

Amphipathic copolymers such as styrene-maleic acid (SMA) have emerged as an important tool to solubilize membrane proteins for structural and functional studies (Figure 3.1.1a).[1–4] The hydrophobic monomer unit inserts into the lipid bilayer to extract the protein in such a way that the protein remains surrounded by a patch of endogenous lipids, often termed SMA lipid particles (SMALPs). A major advantage to using SMA is the ability to directly extract membrane proteins without the need to solubilize with detergent first.

ROS were prepared as described in Chapter 2.1. The membrane pellet was resuspended in Tris buffer [10 mM tris(hydroxymethyl)aminomethane, 100 mM NaCl, pH 8 at 30°C] to obtain a concentration of rhodopsin around 1-1.2 mg/mL (25-30 µM). SMA(3:1) was generously provided by the Farrens lab at Oregon Health and Science University. An appropriate volume of 5% (w/v) SMA(3:1) in Tris buffer was added to

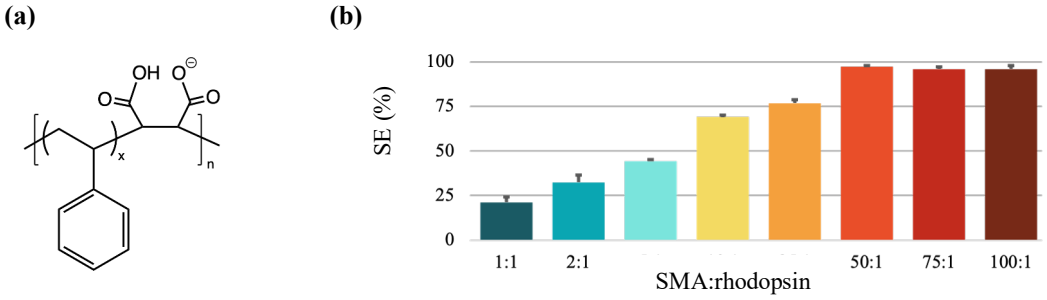

Figure 3.1.1 (a) Chemical structure of styrene-maleic acid (SMA) copolymer at 50% ionization (for SMA(3:1), x ≈ 3, n ≈ 9, and M_n = 10 kDa). **(b)** Percent solubilization efficiency (SE) of SMA(3:1) as a function of the ratio of SMA units per rhodopsin units. Data are averages of 2 independent samples and the positive error value represents the difference in solubilization between both samples.

obtain different molar ratios between SMA and rhodopsin. SMA concentrations were chosen to provide SMA(3:1)/rhodopsin molar ratios of 1, 2, 5, 10, 25, 50, 75, and 100. The sample was mixed well and then centrifuged at 17,000 x g for 20 minutes to isolate the solubilized material (rhodopsin-SMALPs).

Static photobleaching measurements revealed that the amount of rhodopsin solubilized increased as the molar ratio increased up to a value of 50, and above that ratio, the percent solubilized were very similar, ~95% (Figure 3.1.1b). However, excess SMA was found to significantly affect the protein dynamics. Figure 3.1.2 shows the absorption spectra of the rhodopsin-SMALPs (a) pre- and (b) post-photolysis. The rhodopsin-SMALPs prepared at ratios 1, 2, 5, and 10 formed photoproducts that are consistent with an active state composed of ~ 70% Meta II (λ_{max} = 380 nm) and ~30% Meta I_{480} (λ_{max} = 480 nm). Interestingly, the rhodopsin-SMALPs prepared at ratio 25 contained ~55% Meta I_{480} and 45% Meta II, while Meta I_{480} was the only photoproduct formed within rhodopsin-SMALPs prepared at ratios of 50, 75, and 100.

Since Meta I_{480} is expected to be the dominant or only photoproduct recorded if the delay time after illumination is too short to reach the active state, we tested the sample with ratio 50 in more detail. Figure 3.1.3a shows the absorption spectra post-photolysis extended to 45 min with 15-min intervals. There was no noticeable shift in the equilibrium from Meta I_{480} towards Meta II during longer timescales, which indicates that the equilibrium was heavily back-shifted. Instead, the Meta I_{480} present

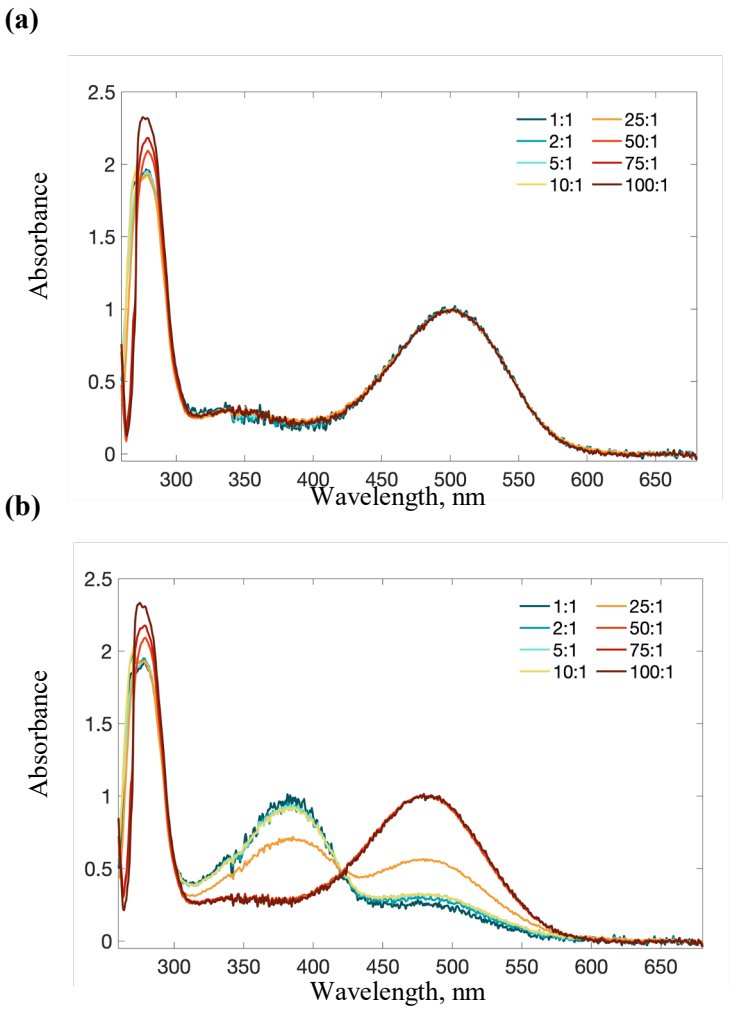

Figure 3.1.2 Static absorption spectra of rhodopsin-SMALPs recorded **(a)** pre- and **(b)** post-photolysis for SMA(3:1)/rhodopsin molar ratios 1 to 100, after being corrected for SMA and light scattering contributions and normalized to 1 A.U. at 500 nm.

post-photolysis gradually converts to a photoproduct that appears slightly blue-shifted. To determine the composition of the final products, 0.9, 0.76, and 0.67 fractions of the Meta I_{480} spectrum measured at 1 minute were subtracted from the spectra recorded at 15, 30, and 45 minutes, respectively, and normalized to 100%. Figure 3.1.3b shows that each spectrum is a mixture of 66% $Meta_{460}$, 27% $Meta_{420}$, and 7% $Meta_{380}$, which are

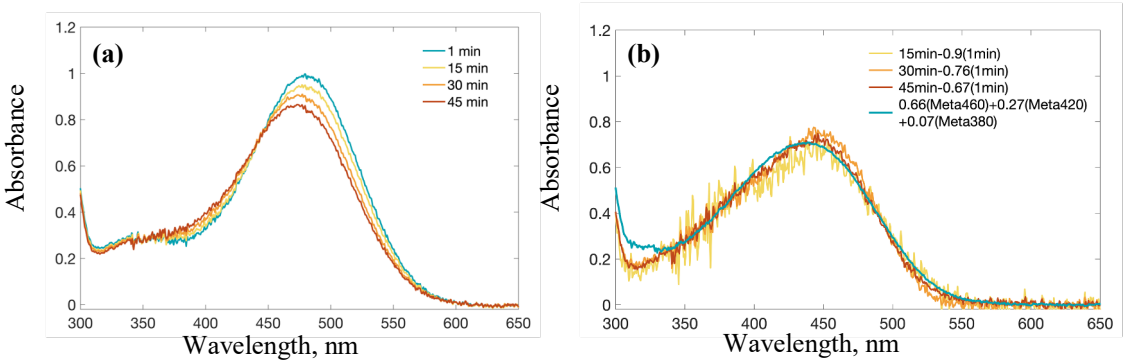

Figure 3.1.3 **(a)** Static absorption spectra at 1-, 15-, 30-, and 45-min post-photolysis for rhodopsin-SMALPs prepared at molar ratio 50. Note that the first curve ~1 min matches Meta I_{480}. **(b)** Absorption spectra of photoproducts from the time-dependent experiment of SMA/rhodopsin molar ratio 50. Fractions of 0.9, 0.76, and 0.67 of the 1-minute spectrum in Figure 3.1.3a were subtracted, and the spectra were normalized to 100%. The blue curve has a final composition of 0.66($Meta_{460}$) + 0.27($Meta_{420}$) + 0.07($Meta_{380}$).

typical spectral forms present in the so-called Meta III intermediate that forms after Meta II.[5] This result implies that rhodopsin stabilized by excess SMA does not reach the active state (Meta II).

We then questioned why these differences are observed in the photoactivation of rhodopsin with samples prepared at high versus low SMA/rhodopsin ratios. One hypothesis was that excess SMA may strip away the lipids surrounding rhodopsin into separate nanoparticles. This is consistent with the light scattering that was observed and corrected for the samples with the absorption spectra shown in Figure 3.1.2. There is a sudden drop in the light scattering of samples with SMA/rhodopsin ratios above 50. Thus, it is clear there is a range of ratios that is optimal for preserving the membrane-like environment during solubilization.

Time-resolved absorption spectroscopy was utilized to investigate the activation mechanism of rhodopsin in an SMA-stabilized environment. The solution pH was set to 8 for efficient solubilization of SMA.[1] Alkaline pH is known to favor the protonated Schiff base forms of rhodopsin, while higher temperature favors the forms with an unprotonated Schiff base.[6,7] Therefore, these experiments were carried out at 30°C to achieve a balance between the two. With an average molecular mass of 10 kDa, we estimated that approximately 10 SMA(3:1) molecules might be needed to form a SMALP with one rhodopsin molecule surrounded by 70 lipid molecules. At an SMA(3:1)/rhodopsin molar ratio of 10 (rS10), the amount of solubilized rhodopsin is roughly 3/4 the maximal value found at the highest ratios.

The time-resolved absorption difference spectra recorded from 1 μs to 2 s at 30°C are shown in Figure 3.1.4a. Global exponential fitting resulted in apparent lifetimes of 85 μs, 2.5 ms, 69 ms, and 0.73 s with the b-spectra displayed in Figure 3.1.4b. The b-spectra were converted into intermediate spectra, and the intermediate spectra were decomposed into sums of the spectral forms as discussed in Chapter 2.5. The experimental absolute spectra produced from the straight sequential scheme (solid lines), along with the reproduced absolute spectra (dashed lines), are displayed in Figure 3.1.4c. The time evolution of the spectral forms is shown in Figure 3.1.4d for rhodopsin in membrane (solid lines) and rhodopsin in rS10 (dashed lines).

Compared to rhodopsin in the native membrane environment, which required fitting only three apparent lifetimes of 70 μs, 0.74 ms and 6.5 ms, the photokinetics of rhodopsin in the rS10 sample were much slower. Rhodopsin in the membrane sample

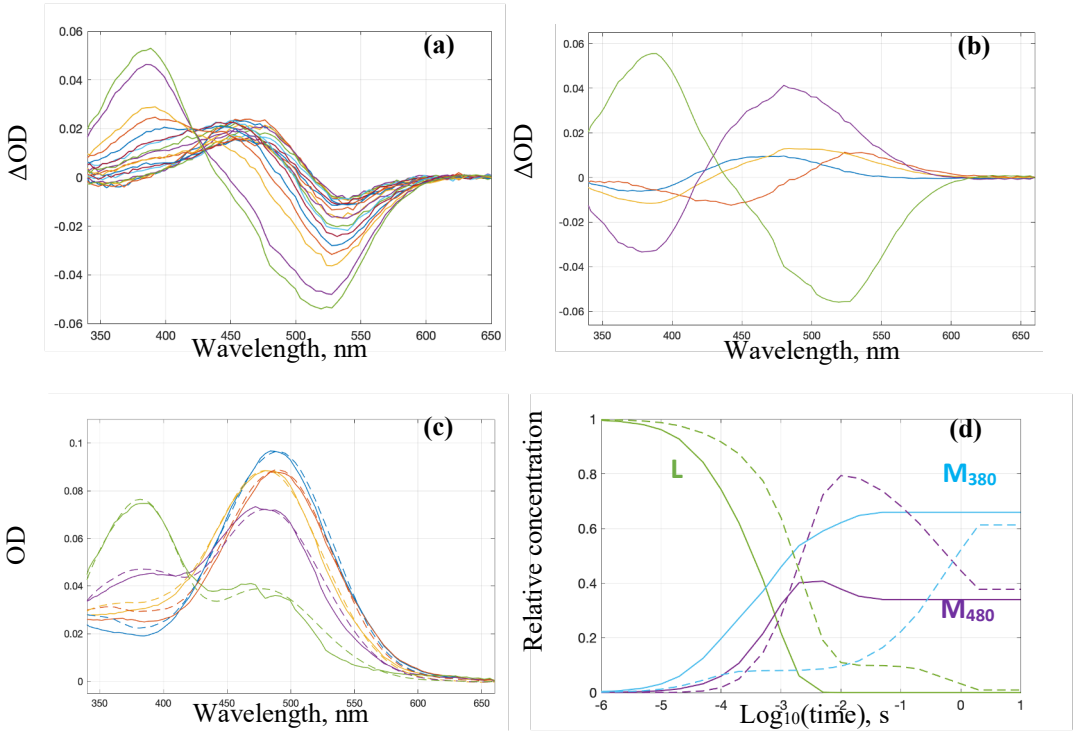

Figure 3.1.4 (a) Light-induced absorption difference spectra of rhodopsin in rS10, recorded from 1 μs to 2 s. **(b)** The b-spectra corresponding to 85 μs (bs_1, blue), 2.5 ms (bs_2, red), 69 ms (bs_3, yellow), 0.73 s (bs_4, purple), and the time-independent final spectrum (bs_0, green), produced by global exponential fit to the time-dependent absorption spectra. **(c)** Absolute spectra of the straight sequential intermediates calculated from the b-spectra (solid lines). The scheme was constructed based on the apparent lifetimes. Reproduction of the absolute spectra using the spectral forms to determine the composition matrix (dashed lines). **(d)** Time evolution of the Lumi (L), $Meta_{480}$ (M_{480}), $Meta_{380}$ (M_{380}) during rhodopsin photoreaction in membrane (solid lines) and rS10 (dashed lines).

shows a branched decay of the Lumi form into $Meta_{480}$ and $Meta_{380}$ forms at early times, followed by an equilibration of $Meta_{480}$–$Meta_{380}$ on the millisecond timescale, which is in an agreement with an earlier report.[6] While it takes rhodopsin less than 10 ms to reach the active state in the membrane, it takes almost a second to do so in the

rS10. An interesting finding is that SMA(3:1) seems to only slow down the reaction steps at the late stages where big conformational and volume changes occur, as the first apparent lifetime (85 μs) is close to what was calculated for the membrane sample (70 μs).

The protonated $Meta_{480}$ spectral form is dominant in rS10, but the unprotonated $Meta_{380}$ spectral form builds up gradually over time. This result suggests that rhodopsin prefers the pathway through the protonated inactive forms over the unprotonated ones. Even though rhodopsin in rS10 completes a slower kinetic path that is different from what is observed in the membrane, it still reaches the final active state. Both final states of rhodopsin in the membrane and rS10 contained the $Meta_{480}$ and $Meta_{380}$ spectral forms in a ~1:2 ratio, which is characteristic of the equilibrium between $Meta_{480}$ and the active state Meta II at 30°C.[6] However, this equilibrium must have been reached differently since the number of apparent rates in the rS10 is one more than in the membrane. Since rhodopsin in the SMALP takes one more step to cover the path from Lumi to the active state, there are likely two Meta I_{480} states in the reaction sequence. The extra step and intermediate requires an extended model, the double-square scheme, to describe the kinetics. The presence of an additional intermediate in the straight sequential scheme confirms that the classical square model is not a valid representation of rhodopsin kinetics at ambient temperature.[8]

The kinetic picture deduced for the rS10 sample applies to SMALPs made at lower SMA(3:1)/rhodopsin molar ratios. The results presented in Figure 3.1.2 showed that the samples with low ratios have the same spectral composition up to 1 min after

photobleaching. To obtain insight on the kinetics at lower molar ratios, time-resolved absorption difference spectra were measured for rhodopsin-SMALPs prepared at ratio 5. The results showed only slight deviations, that were within the limits of reproducibility, from the kinetics for rS10. Thus, it is likely that rhodopsin-SMALPs made at ratios that do not exceed 10-15 resemble the structure reported by T.R. Dafforn and colleagues.[9] Notably, the molar ratio of 10-15 roughly corresponds to the 1.2:1 SMA/lipid mass ratio required for complete solubilization of lipid membranes.[10]

Rhodopsin-SMALPs formed with SMA(3:1)/rhodopsin molar ratios of 20 (rS20) showed a very different activation pathway. The time-resolved absorption difference spectra for rS20 recorded at delay times 1 μs to 20 s are displayed in Figure 3.1.5a. Global exponential fitting revealed four apparent lifetimes of 0.26 ms, 12 ms, 0.78 s, and 6.4 s with the b-spectra shown in Figure 3.1.5b. As suggested by the static photobleaching experiments, rhodopsin-SMALPs formed with SMA(3:1)/rhodopsin molar ratios of 100 (rS100) deviated from the kinetic path even more so than the rS20 sample. The time-resolved absorption difference spectra for rS100 recorded from 1 μs to 10 s are shown in Figure 3.1.5c. Although the accuracy of the data is lower compared to the other samples, it was clear that significant spectral changes only occur at late times. Two apparent lifetimes, 56 ms and 3.2 s, were fitted to the data with the b-spectra shown in Figure 3.1.5d.

The experimental absolute spectra from the straight sequential scheme (solid lines) for rhodopsin in rS20, and the reproduced absolute spectra (dashed lines), are displayed in Figure 3.1.6a. The analogous spectra for the rS100 sample are shown in

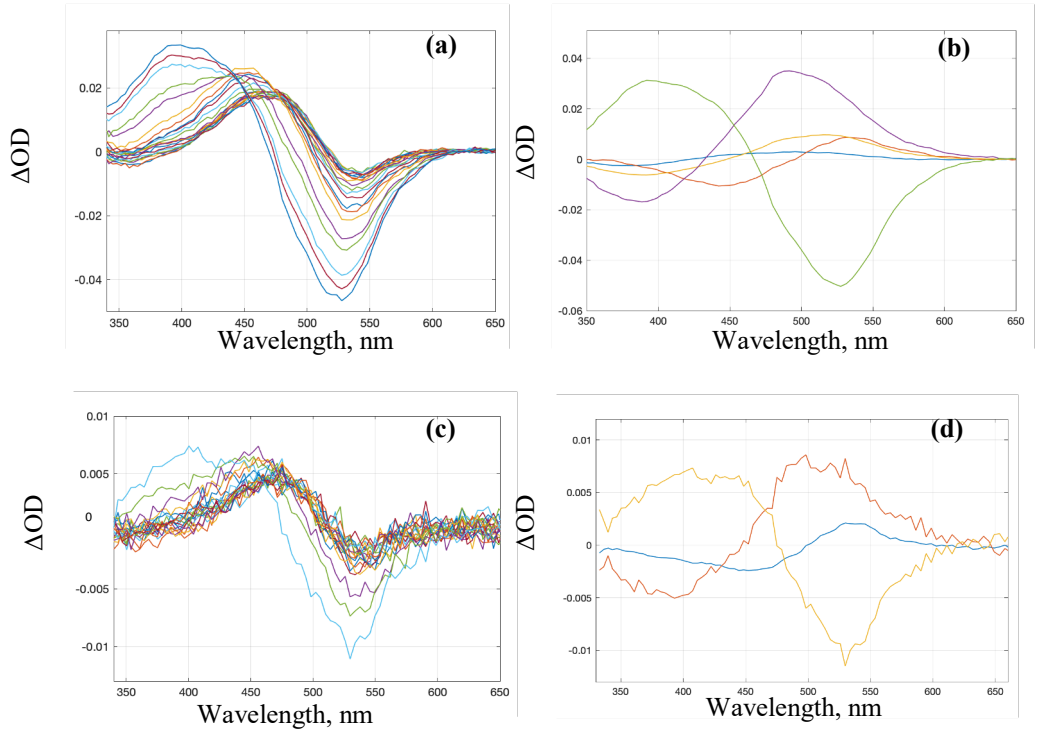

Figure 3.1.5 (a) Light-induced absorption difference spectra of rhodopsin in rS20, recorded from 1 µs to 20 s. **(b)** The b-spectra corresponding to 0.26 ms (bs_1, blue), 12 ms (bs_2, red), 0.78 ms (bs_3, yellow), 6.4 s (bs_4, purple), and the time-independent final spectrum (bs_0, green), produced by global exponential fit to the time-dependent absorption spectra. **(c)** Light-induced absorption difference spectra of rhodopsin in rS100, recorded from 1 µs to 10 s. **(d)** The b-spectra corresponding to 56 ms (bs_1, blue), 3.2 ms (bs_2, red), and the time-independent final spectrum (bs_0, yellow), produced by global exponential fit to the time-dependent absorption spectra.

Figure 3.1.6b. The time evolution of the spectral forms shown in Figure 3.1.6c compares rhodopsin in rS20 (solid lines) and rS100 (dashed lines). Rhodopsin in rS20 exhibits very slow kinetics and the composition of the final intermediate is substantially different from the one seen in the membrane sample. No combination of $Meta_{480}$ and $Meta_{380}$ spectral forms could reproduce the last absolute spectrum (Figure 3.1.6a, solid green line). An additional spectral form with λ_{max} at 460 nm, $Meta_{460}$, was required.

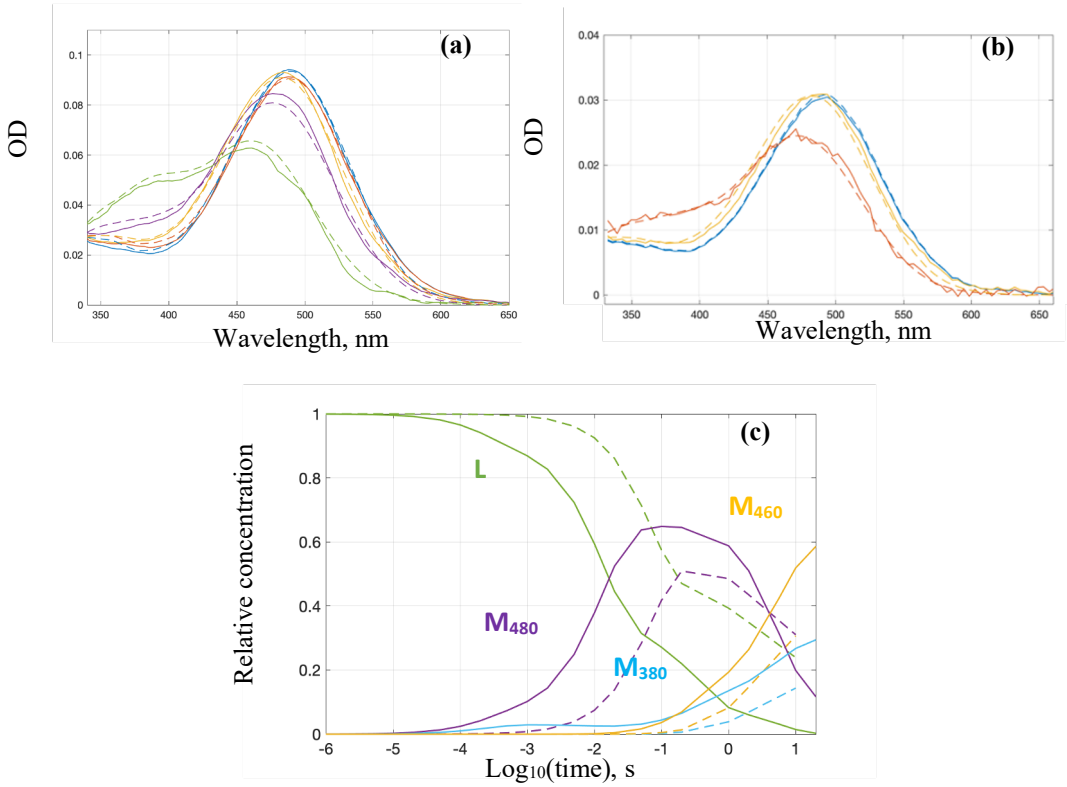

Figure 3.1.6 (a) Absolute spectra of the straight sequential intermediates calculated from the b-spectra of rhodopsin in rS20 (solid lines). The scheme was constructed based on the apparent lifetimes. Reproduction of the absolute spectra by the model spectra to determine the spectral compositions (dashed lines). **(b)** Absolute spectra of the straight sequential intermediates calculated from the b-spectra of rhodopsin in rS100 (solid lines). The scheme was constructed based on the apparent lifetimes. Reproduction of the absolute spectra using the spectral forms to determine the composition matrix (dashed lines). **(c)** Time evolution of the Lumi (L), $Meta_{480}$ (M_{480}), $Meta_{460}$ (M_{460}), $Meta_{380}$ (M_{380}) during rhodopsin photoreaction in rS20 (solid lines) and rS100 (dashed lines).

$Meta_{460}$ is a protonated spectral form that is detected on the seconds-to-minutes timescale during the deactivation of rhodopsin.[5]

The time evolution of rhodopsin in rS20 shows that around 65% of the Lumi spectral form decays into $Meta_{480}$, while 2-3% decays into $Meta_{380}$. Around 1 s, more

$Meta_{380}$ is formed from both Lumi and $Meta_{480}$. However, this buildup is accompanied by the formation of twice as much $Meta_{460}$, which is a spectral form that is not part of the kinetic pathways leading to the active state. Rhodopsin in rS100 displays even slower kinetics. Additionally, the time evolution of rS100 has practically a single transition between Lumi and $Meta_{480}$ from 10 ms to 100 ms before the onset of $Meta_{460}$ around 300 ms (Figure 3.1.6c, dashed lines). Since analyzing distorted or fragmented kinetic models is outside the scope of this work, the kinetic analysis of the rS20 and the rS100 samples was not pursued further.

3.2 Removal of Excess Polymer

An ideal solubilizing agent is one that extracts nearly all of the protein without distorting the activation mechanism. With rhodopsin-SMALPs, only molar ratios of SMA(3:1)/rhodopsin that were 50 or higher extracted more than 90% of the protein. However, the spectral data for rhodopsin in rS20 and rS100 showed very distorted photokinetics that did not "reach" the active state. Since we ultimately want to measure the kinetics of costly recombinant rhodopsin samples, we wanted to test if the altered protein dynamics at high SMA concentration were reversible. Could we extract a larger yield of protein with high SMA concentration and then remove the excess SMA(3:1) to restore the rhodopsin photokinetics observed in rS10?

ROS samples were prepared as described in Chapter 2.1. After centrifuging the sample for 20 minutes at 17,000 x g, the membrane pellet was resuspended in Tris buffer [10 mM tris(hydroxymethyl)aminomethane, 100 mM NaCl, pH 8 at 30°C] to

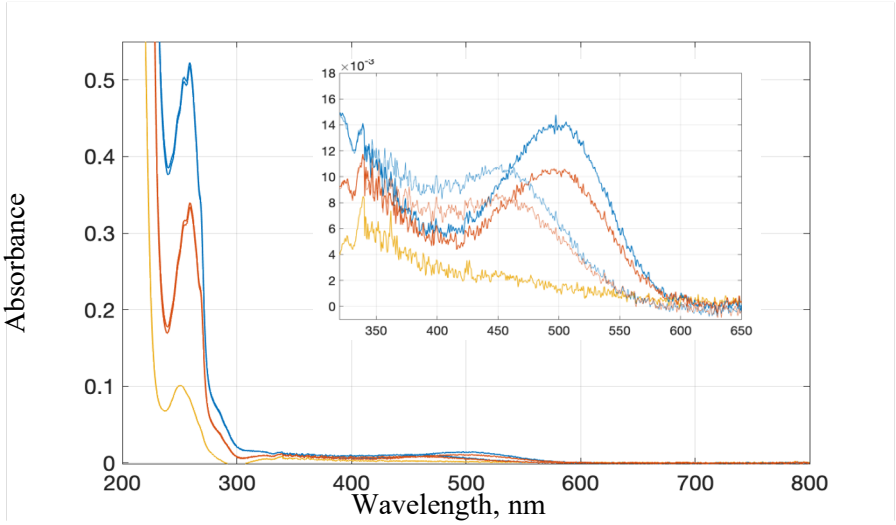

Figure 3.2.1 Static absorption spectra of rhodopsin-SMALPs during the removal of excess SMA(3:1). The blue traces are the sample after rhodopsin was solubilized with SMA at a molar ratio of 100. The red traces are the sample after the excess SMA was removed with the MWCO centrifugal filter. The yellow trace is the wash that passed through the MWCO centrifugal filter. The inset shows that the rhodopsin-SMALPs did not pass through the filter.

obtain a concentration of rhodopsin around 0.9 mg/mL (22 µM). An appropriate volume of 5% (w/v) SMA(3:1) in Tris buffer was added to obtain a molar ratio of 100 SMA/rhodopsin. The sample was mixed well and then centrifuged at 17,000 x g for 20 minutes to isolate the solubilized material. The solubilized fraction was added to a 30K molecular weight cut-off (MWCO) centrifugal filter and centrifuged at 8,000 x g for 20 minutes. The material that did not pass through the filter was resuspended with a small volume of Tris buffer. The final concentration of rhodopsin was 0.4 mg/mL (~10 µM), so less than half of the original amount of rhodopsin was solubilized with SMA(3:1) and subsequently recovered from the MWCO filter. The absorbance of the wash that passed through the MWCO filter was also measured to confirm that excess

SMA(3:1), with λ_{max} at 260 nm, was removed from the sample (Figure 3.2.1).

Time-resolved absorption difference spectra recorded from 1 µs to 10 s at 30°C are displayed in Figure 3.2.2. Comparing the photolysis products before (Figure 3.1.5c) and after the excess SMA was removed (Figure 3.2.2) shows no spectral difference and that the active state was not restored. This indicated that the amount of SMA added in excess of the minimal amount required for solubilization causes changes to the rhodopsin environment that are not reversible. This experiment also demonstrates that it is not feasible to extract a higher yield of protein and then remove the excess polymer since a fairly large portion of the sample gets lost on the MWCO filter.

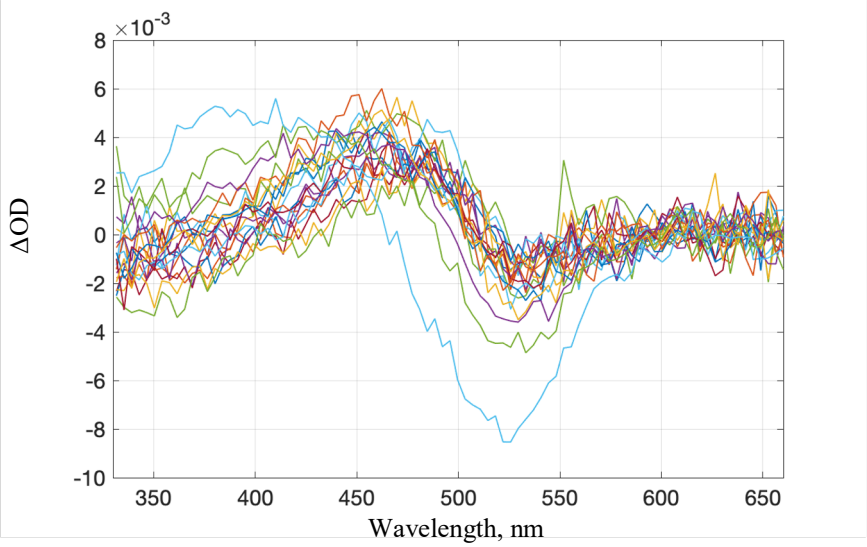

Figure 3.2.2. Light-induced absorption difference spectra of rhodopsin in rS100 SMALPs after excess SMA was removed with a MWCO centrifugal filter, recorded from 1 µs to 10 s.

3.3 Dilute Styrene Maleic Acid Lipid Particle Samples

It is clear that high SMA concentrations cause structural changes to the protein that are not reversible. Hence, we wanted to test what was the minimum amount of rhodopsin-SMALPs required to obtain kinetic data for the spectral analysis. The preparation of recombinant rhodopsin samples to study mutations relevant to retinal disease takes time, is expensive, and does not result in high yields after the work-up procedure. Thus, it is important to compare the results obtained with low sample concentrations to those collected at higher concentrations.

ROS samples were prepared as described in Chapter 2.1. The membrane pellet was resuspended in Tris buffer [10 mM tris(hydroxymethyl)aminomethane, 100 mM NaCl, pH 8 at 30°C] to obtain a concentration of rhodopsin around 1.8 mg/mL (44 μM). An appropriate volume of 5% (w/v) SMA(3:1) in Tris buffer was added to obtain a molar ratio of 10 SMA/rhodopsin. The sample was mixed well and then centrifuged at 17,000 x g for 20 minutes to isolate the solubilized material. The rhodopsin concentration in the solubilized fraction was determined. Small volumes of the solubilized fraction were diluted with Tris buffer to prepare two samples at 400 μg/mL. One of the two samples was divided in half and diluted with Tris buffer to provide two samples at 200 μg/mL.

Time-resolved absorption difference spectra recorded from 1 μs to 2 s at 30°C for the sample with 400 μg rhodopsin/mL are displayed in Figure 3.3.1a. Global exponential fitting resulted in apparent lifetimes of 0.11 ms, 2.3 ms, 71 ms, and 0.99 s with the b-spectra displayed in Figure 3.3.1b. Time-resolved absorption difference

spectra recorded from 1 µs to 2 s at 30°C for the average of two samples with 200 µg rhodopsin/mL are displayed in Figure 3.3.1c. Global exponential fitting resulted in apparent lifetimes of 0.10 ms, 2.0 ms, 61 ms, and 0.76 s with the b-spectra displayed in Figure 3.3.1d.

Overall, the data sets are similar to the results for rhodopsin in the rS10 sample prepared at a higher concentration (~1 mg/mL) discussed above in Section 3.1.

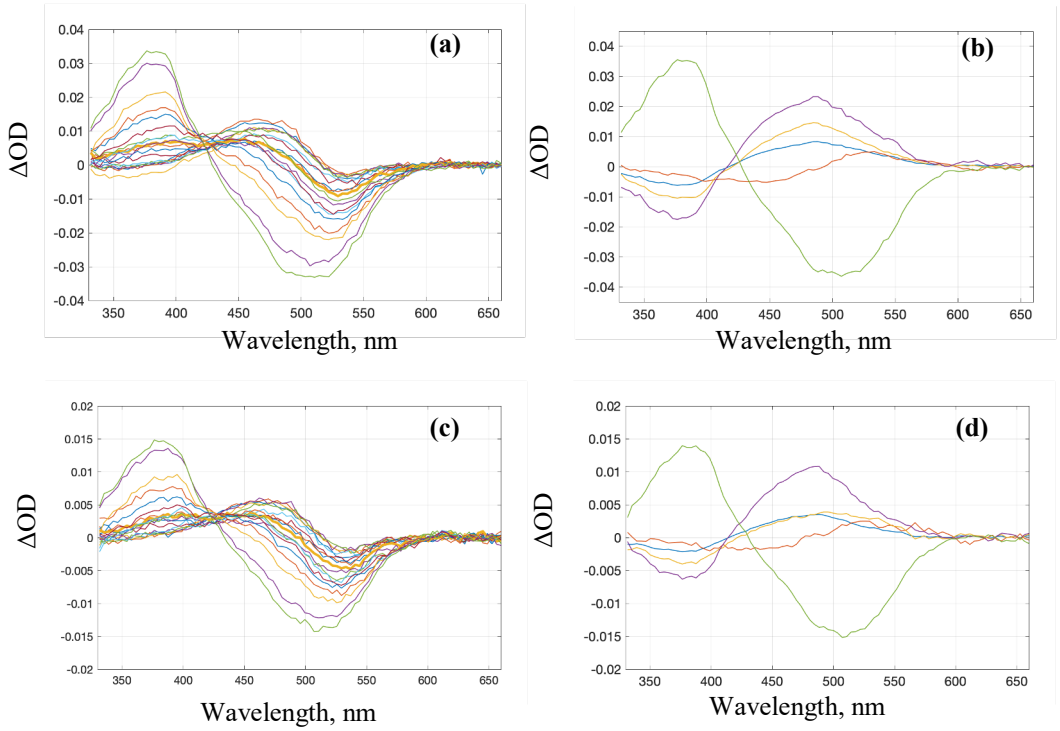

Figure 3.3.1 (a) Light-induced absorption difference spectra of one sample of 400 µg/mL rhodopsin in rS10, recorded from 1 µs to 2 s. **(b)** The b-spectra corresponding to 0.11 ms (bs_1, blue), 2.3 ms (bs_2, red), 71 ms (bs_3, yellow), 0.99 s (bs_4, purple), and the time-independent final spectrum (bs_0, green), produced by global exponential fit to the time-dependent absorption spectra. **(c)** Light-induced absorption difference spectra from an average of two samples of 200 µg/mL rhodopsin in rS10, recorded from 1 µs to 2 s. **(d)** The b-spectra corresponding to 0.10 ms (bs_1, blue), 2.0 ms (bs_2, red), 61 ms (bs_3, yellow), 0.76 s (bs_4, purple), and the time-independent final spectrum (bs_0, green), produced by global exponential fit to the time-dependent absorption spectra.

However, based on the signal-to-noise ratios of the experimental difference spectra for the samples with low concentration, we determined it would be best to obtain one data set from a sample with ~400 μg/ml of rhodopsin as opposed to combining two data sets from rhodopsin samples at ~200 μg/ml. With the time-resolved optical absorption measurements and our method of analyzing data, it is often better to have a larger signal size and fewer averages than a smaller signal size and more averages.

3.4 Addition of Phosphatidylcholine Liposomes

The Meta I_{480}–Meta II transition involves movement of the protein helices, which requires a fluid lipid environment.[11,12] From the results presented in Section 3.1, we hypothesized that the high SMA/rhodopsin ratios cause an increased rigidity of rhodopsin and its surroundings, such that the Meta I_{480}–Meta II equilibrium becomes heavily back-shifted. To test how lipid fluidity influences rhodopsin photokinetics in SMALPs, phosphatidylcholine (PC) liposomes were prepared and added to the samples. First, 0.015 g of L-α-phophatidylcholine was added to a scintillation vial and dissolved using ~2 mL of chloroform. The solvent was evaporated using a gentle stream of nitrogen gas in a fume hood. The lipid film dried overnight, and then was resuspended in 1 mL of Tris buffer [10 mM tris(hydroxymethyl)aminomethane, 100 mM NaCl, pH 8 at 30°C]. The solution was transferred to an Eppendorf tube and sonicated for 1 minute with 15 second on/off intervals. An aliquot (150 μL) of the liposome solution was transferred to another Eppendorf tube, and 5% (w/v) SMA(3:1) in Tris buffer was added in 10 μL increments until the solution became noticeably

transparent (30 µL total).

ROS samples were prepared as described in Chapter 2.1. The ROS was centrifuged at 17,000 x g for 20 minutes, and then the membrane pellet was resuspended in Tris buffer [10 mM tris(hydroxymethyl)aminomethane, 100 mM NaCl, pH 8 at 30°C] to obtain a concentration of rhodopsin that measured 1.75 mg/mL (43 µM). A small volume (572 µL) of the rhodopsin was transferred to the liposome-SMA solution, mixed well, and then left at room temperature for a few minutes. The sample contained a total of 2.25 mg lipid:1.5 mg SMA:1 mg rhodopsin, and the molar ratio of SMA/rhodopsin was 6 (rS6pc). The sample was centrifuged at 17,000 x g for 20 minutes, and the soluble fraction was isolated for further analysis.

Time-resolved absorption difference spectra recorded from 1 µs to 2 s at 30°C are displayed in Figure 3.4.1a. Global exponential fitting revealed four apparent lifetimes of 49 µs, 0.81 ms, 13 ms, and 0.15 s with the b-spectra shown in Figure 3.4.1b. The experimental absolute spectra (solid lines), along with the reproduced absolute spectra (dashed lines), are displayed in Figure 3.4.1c. The time evolution of spectral forms shown in Figure 3.4.1d compares rhodopsin in membrane (solid lines) and rhodopsin in rS6pc (dashed lines).

Based on the b-spectra and the absolute spectra of the intermediates, it is clear that more of the unprotonated spectral form ($Meta_{380}$) is formed upon addition of the PC liposomes. The rhodopsin does not exhibit preference for the reaction pathway of the protonated forms. Considering that the Meta I_{480}–Meta II transition involves motions of the protein helices and requires a fluid lipid environment, this result

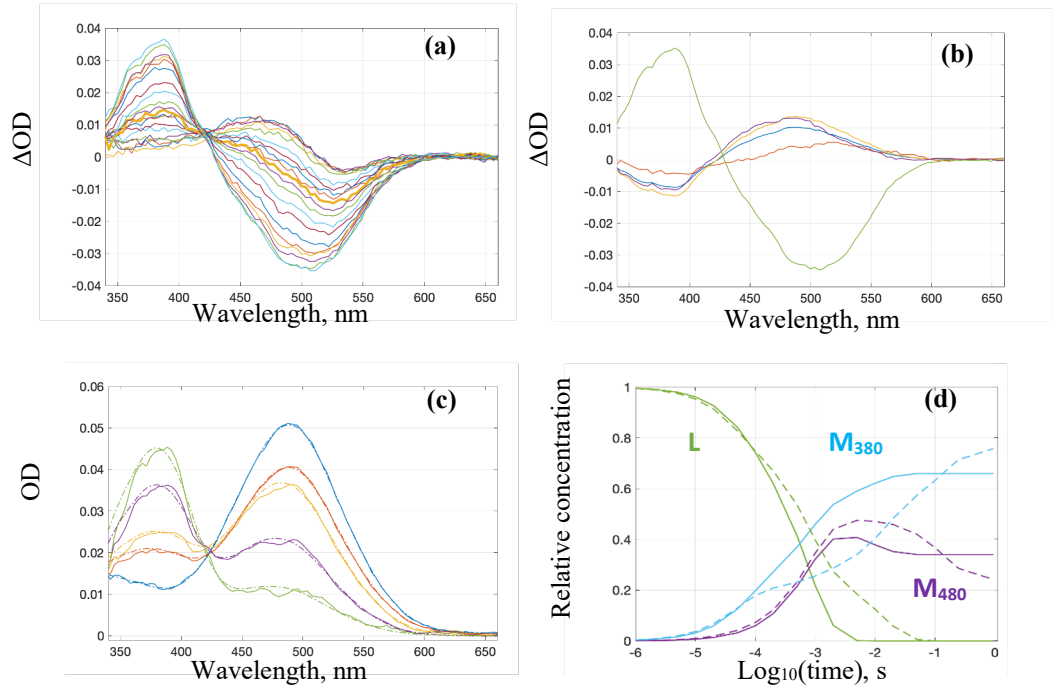

Figure 3.4.1 (a) Light-induced absorption difference spectra of rhodopsin in rS6pc SMALPs, recorded from 1 µs to 2 s. **(b)** The b-spectra corresponding to 49 µs (bs_1, blue), 0.81 ms (bs_2, red), 13 ms (bs_3, yellow), 0.15 s (bs_4, purple), and the time-independent final spectrum (bs_0, green), produced by global exponential fit to the time-dependent absorption spectra. **(c)** Absolute spectra of the straight sequential intermediates calculated from the b-spectra (solid lines). The scheme was constructed based on the apparent lifetimes. Reproduction of the absolute spectra using the spectral forms to determine the composition matrix (dashed lines). **(d)** Time evolution of the Lumi (L), $Meta_{480}$ (M_{480}), $Meta_{380}$ (M_{380}) during rhodopsin photoreaction in membrane (solid lines) and rS6pc (dashed lines).

suggests that the liposomes introduce fluidity to the SMALP system. It is interesting to note that higher temperature, which increases the fluidity of the lipid environment, also favors the reaction pathway of the unprotonated forms.[6]

3.5 Variation in the Styrene/Maleic Acid Monomer Ratio

The spectral analysis of rhodopsin in rS10 presented in Figure 3.1.4 showed that SMA(3:1) copolymer slows down the reaction steps at the late stages where big conformational changes occur. The slow rates can be explained in a few ways. One hypothesis is that the insertion of the hydrophobic styrene blocks of the copolymer between the unsaturated lipid acyl chains causes the lipid environment to increase in rigidity. Increasing the rigidity would slow down or even prevent the protein conformation changes necessary for the reaction to progress, similar to what happens by lowering the temperature.[7] Another hypothesis for the slow rates observed in rhodopsin-SMALPs is that the hydrophobic moieties of the polymer are interacting with the proposed cholesterol binding site of the inactive conformation, which would slow down the movement of the helices required to reach the active state.[13,14] To investigate how the hydrophobicity of the copolymer influences the photokinetics of rhodopsin, other variations of SMA were tested.

ROS were prepared as described in Chapter 2.1. The membrane pellet was resuspended in Tris buffer [10 mM tris(hydroxymethyl)aminomethane, 100 mM NaCl, pH 8 at 30°C] to obtain a concentration of rhodopsin around 0.9-1.3 mg/mL (22-32 μM). SMA(2:1) was purchased from Anatrace, and SMA(1.2:1) was generously provided by the Long lab at University of Tennessee at Knoxville. An appropriate volume of 5% (w/v) SMA(2:1) or 10% (w/v) SMA(1.2:1) in Tris buffer were added to obtain low molar ratios (5-10) of SMA/rhodopsin. The samples were mixed well and then centrifuged at 17,000 x g for 20 minutes to isolate the solubilized material.

The time-resolved absorption difference spectra recorded from 1 μs to 2 s at 30°C for the SMA(2:1) sample are shown in Figure 3.5.1a. Global exponential fitting resulted in apparent lifetimes of 52 μs, 1.8 ms, 45 ms, and 0.37 s with the b-spectra displayed in Figure 3.5.1b. The time-resolved absorption difference spectra recorded from 1 μs to 2 s at 30°C for the SMA(1.2:1) sample are shown in Figure 3.5.1c. Global exponential fitting resulted in apparent lifetimes of 43 μs, 1.5 ms, 28 ms, and 0.74 s with the b-spectra displayed in Figure 3.5.1d.

The second b-spectrum of the rhodopsin in low ratio SMALPs prepared with SMA(3:1) (Figure 3.1.4b, red line) doesn't show any 380 nm photoproduct, as indicated by the lack of a negative ΔOD at 380 nm, which suggests that the Meta I_{380} formed in the first step decays into Meta I_{480} before formation of Meta II. However, the second b-spectrum for both samples of rhodopsin in low ratio SMALPs prepared with SMA(2:1) and SMA(1.2:1) show a small amount of the 380 nm photoproduct (Figures 3.5.1b and 3.5.1d, red line). Furthermore, the 480 nm to 380 nm transition, noted by a positive ΔOD at 480 nm and a negative ΔOD at 380 nm, has a smaller amplitude in the third b-spectrum compared to the fourth b-spectrum for the sample with SMA(3:1) (Figure 3.5.1b, yellow and purple lines, respectively). This suggests that most of the deprotonated intermediate needed to reach the active state is formed during the last step, around 1 second. On the contrary, the third b-spectrum in the sample with SMA(1.2:1) has a larger amplitude than the fourth b-spectrum (Figure 3.5.1d, yellow and purple lines, respectively), so most of the deprotonated intermediate forms in tens of milliseconds instead.

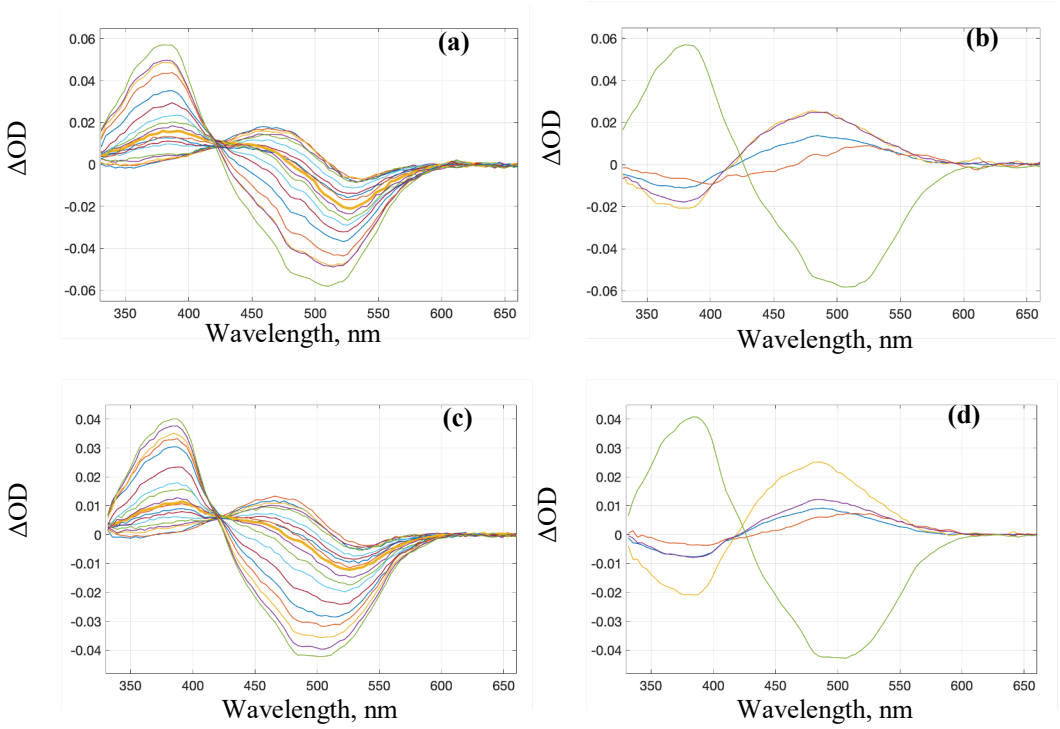

Figure 3.5.1 (a) Light-induced absorption difference spectra of rhodopsin in low ratio SMALPs prepared with SMA(2:1), recorded from 1 µs to 2 s. **(b)** The b-spectra corresponding to 52 µs (bs_1, blue), 1.8 ms (bs_2, red), 45 ms (bs_3, yellow), 0.37 s (bs_4, purple), and the time-independent final spectrum (bs_0, green), produced by global exponential fit to the time-dependent absorption spectra. **(c)** Light-induced absorption difference spectra of rhodopsin in low ratio SMALPs prepared with SMA(1.2:1), recorded from 1 µs to 2 s. **(d)** The b-spectra corresponding to 43 µs (bs_1, blue), 1.5 ms (bs_2, red), 28 ms (bs_3, yellow), 0.74 s (bs_4, purple), and the time-independent final spectrum (bs_0, green), produced by global exponential fit to the time-dependent absorption spectra.

Low styrene content results in an increasing amount of $Meta_{380}$ formed earlier in the reaction, which indicates that there is less rigidity surrounding rhodopsin or less interaction with the cholesterol binding site. This means that there is less preference for the pathway through the protonated inactive forms and is thus an improvement from SMALPs prepared with high styrene content. However, the different ratios of

styrene/maleic acid do not appear to have a major effect on the apparent rates that correspond to the b-spectra of the straight sequential scheme, and the reaction steps at the late stages are still very slow. While the use of SMALPs has a big advantage of avoiding the use of detergents, this work with rhodopsin suggests that optimal SMA conditions must be established for kinetic and dynamic membrane protein studies.

3.6 References

(1) Scheidelaar, S.; Koorengevel, M. C.; van Walree, C. A.; Dominguez, J. J.; Dörr, J. M.; Killian, J. A. Effect of Polymer Composition and PH on Membrane Solubilization by Styrene-Maleic Acid Copolymers. *Biophys. J.* 2016, *111* (9), 1974–1986. https://doi.org/10.1016/j.bpj.2016.09.025.

(2) Broecker, J.; Eger, B. T.; Ernst, O. P. Crystallogenesis of Membrane Proteins Mediated by Polymer-Bounded Lipid Nanodiscs. *Structure* 2017, *25* (2), 384–392. https://doi.org/10.1016/j.str.2016.12.004.

(3) Overduin, M.; Esmaili, M. Structures and Interactions of Transmembrane Targets in Native Nanodiscs. *SLAS Discov.* 2019, *24* (10), 943–952. https://doi.org/10.1177/2472555219857691.

(4) Skrzypek, R.; Iqbal, S.; Callaghan, R. Methods of Reconstitution to Investigate Membrane Protein Function. *Methods* 2018, *147*, 126–141. https://doi.org/10.1016/j.ymeth.2018.02.012.

(5) Szundi, I.; Lewis, J. W.; Kuijk, F. J. G. M. van; Kliger, D. S. Effect of NADPH on Formation and Decay of Human Metarhodopsin III at Physiological Temperatures. *Vision Res* 2000, *40* (22), 3039–3048. https://doi.org/10.1016/s0042-6989(00)00148-6.

(6) Thorgeirsson, T. E.; Lewis, J. W.; Wallace-Williams, S. E.; Kliger, D. S. Effects of Temperature on Rhodopsin Photointermediates from Lumirhodopsin to Metarhodopsin II. *Biochemistry* 1993, *32* (50), 13861–13872. https://doi.org/10.1021/bi00213a015.

(7) Matthews, R. G.; Hubbard, R.; Brown, P. K.; Wald, G. Tautomeric Forms of Metarhodopsin. *J. Gen. Physiol.* 1963, *47* (2), 215–240. https://doi.org/10.1085/jgp.47.2.215.

(8) Szundi, I.; Funatogawa, C.; Kliger, D. S. Complexity of Bovine Rhodopsin Activation Revealed at Low Temperature and Alkaline PH. *Biochemistry* 2016, *55* (36), 5095–5105. https://doi.org/10.1021/acs.biochem.6b00687.

(9) Jamshad, M.; Grimard, V.; Idini, I.; Knowles, T. J.; Dowle, M. R.; Schofield, N.; Sridhar, P.; Lin, Y.; Finka, R.; Wheatley, M.; Thomas, O. R. T.; Palmer, R. E.; Overduin, M.; Govaerts, C.; Ruysschaert, J.-M.; Edler, K. J.; Dafforn, T. R. Structural Analysis of a Nanoparticle Containing a Lipid Bilayer Used for Detergent-Free Extraction of Membrane Proteins. *Nano Res* 2014, *8* (3), 774–789. https://doi.org/10.1007/s12274-014-0560-6.

(10) Zhang, R.; Sahu, I. D.; Liu, L.; Osatuke, A.; Comer, R. G.; Dabney-Smith, C.; Lorigan, G. A. Characterizing the Structure of Lipodisq Nanoparticles for Membrane Protein Spectroscopic Studies. *BBA-Biomembranes* 2015, *1848* (1), 329–333. https://doi.org/10.1016/j.bbamem.2014.05.008.

(11) Farrens, D. L.; Altenbach, C.; Yang, K.; Hubbell, W. L.; Khorana, H. G. Requirement of Rigid-Body Motion of Transmembrane Helices for Light Activation of Rhodopsin. *Science* 1996, *274* (5288), 768–770. https://doi.org/10.1126/science.274.5288.768.

(12) Ahuja, S.; Hornak, V.; Yan, E. C. Y.; Syrett, N.; Goncalves, J. A.; Hirshfeld, A.; Ziliox, M.; Sakmar, T. P.; Sheves, M.; Reeves, P. J.; Smith, S. O.; Eilers, M. Helix Movement Is Coupled to Displacement of the Second Extracellular Loop in Rhodopsin Activation. *Nat. Struct. Mol. Biol.* 2009, *16* (2), 168–175. https://doi.org/10.1038/nsmb.1549.

(13) Albert, A. D.; Boesze-Battaglia, K. The Role of Cholesterol in Rod Outer Segment Membranes. *Prog Lipid Res* 2005, *44* (2–3), 99–124. https://doi.org/10.1016/j.plipres.2005.02.001.

(14) Sejdiu, B. I.; Tieleman, D. P. Lipid-Protein Interactions Are a Unique Property and Defining Feature of G Protein-Coupled Receptors. *Biophys. J.* 2020, *118* (8), 1887–1900. https://doi.org/10.1016/j.bpj.2020.03.008.

CHAPTER 4 Rhodopsin Solubilized in Other Systems

4.1 Functionalized SMA Copolymers

SMA copolymers functionalized with alkoxy ethoxylate and ethylene glycol sidechains have been synthesized to investigate how SMA functionalization alters the extraction efficiency of specific proteins (Figure 4.1.1). Recently, the laboratories of Barry Bruce and Brian Long found that the solubilization of photosystem I (PSI) from the thylakoid membranes of cyanobacterium *Thermosynechococcus elongatus* (*Te*) depended on the length of the sidechain and extent of esterification.[1] In general, longer alkoxy ethoxylate sidechains resulted in single, trimeric PSI-SMALPs with high yield, while short sidechains resulted in a lower yield. Also, the more hydrophobic polymers have higher solubilization efficiencies, particularly at high percentages of esterification. In contrast, unfunctionalized SMA resulted in large, PSI-containing membrane patches with very low yield.

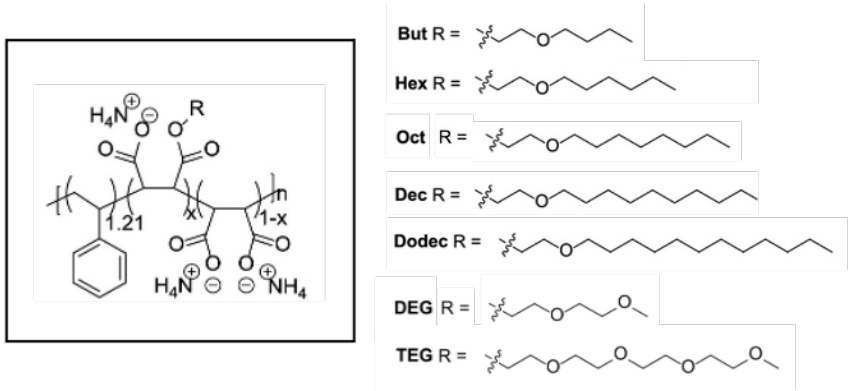

Figure 4.1.1 Functionalized SMA copolymers – alkoxy ethoxylate sidechains (But, Hex, Oct, Dec, Dodec) and ethylene glycol sidechains (DEG, TEG) with x equal to percent esterified. Ex. 23% esterification means 23% anhydride groups are functionalized while 77% remain unfunctionalized.

Rhodopsin was used as a tool to study how these functionalized SMA copolymers influence the extraction efficiency of protein from a phospholipid-rich environment. ROS were prepared as described in Chapter 2.1. The membrane pellet was resuspended in Tris buffer [10 mM tris(hydroxymethyl)aminomethane, 100 mM NaCl, pH 7.8 at room temperature] to obtain a concentration of rhodopsin around 0.9 mg/mL (22 μM). Functionalized SMA copolymers were generously provided by the Long lab at University of Tennessee, Knoxville. A small volume of 15% (w/v) functionalized SMA copolymer in Tris buffer was added to an aliquot of hypotonically washed ROS that contained ~1 mg/mL rhodopsin to achieve a final concentration of 1.5% (w/v) copolymer. The samples were mixed well and then centrifuged at 17,000 x g for 20 minutes to isolate the solubilized material. Static photobleaching measurements were conducted as described in Chapter 2.2.

Figure 4.1.2 shows the percent solubilization efficiency (SE) as a function of percent esterification for the functionalized SMA polymers. The SE of rhodopsin was between 85-100% for the alkoxy ethoxylate SMA copolymers But, Hex, and Oct, regardless of the percent esterification. The alkoxy ethoxylate polymers that have longer sidechain lengths, Dec and Dodec, extracted a significant amount of rhodopsin at 23% esterification. However, the amount of rhodopsin solubilized by Dec and Dodec decreases at 30-35% esterification, but then increases again at 52% esterification. A similar, but less dramatic, trend was observed when extracting PSI from thylakoid membranes with Dodec.[1] It is not clear what causes this observation. A replicate

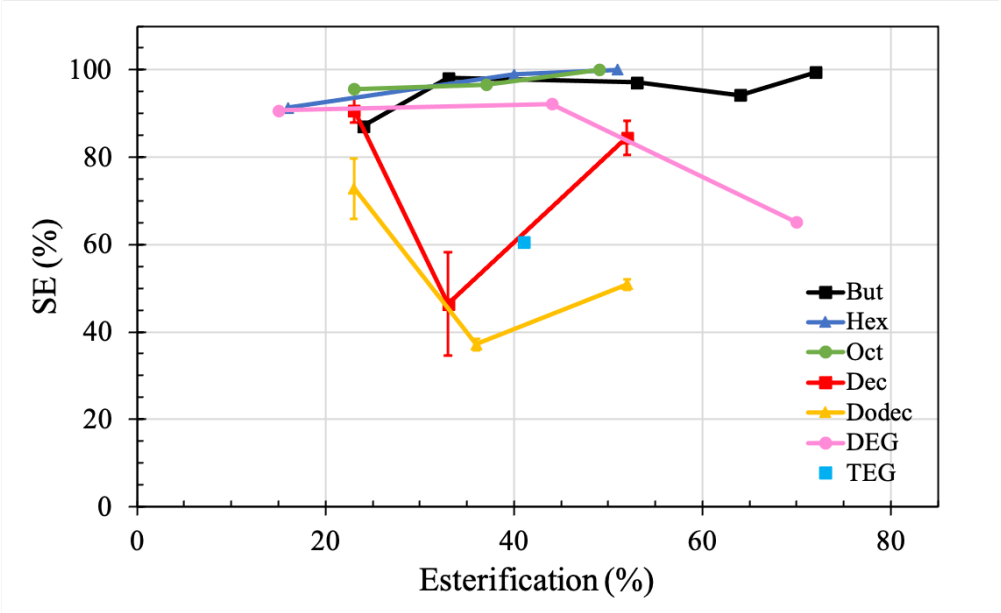

Figure 4.1.2 Percent solubilization efficiency (SE) as a function of percent esterification for the series of functionalized SMA copolymers. For Dec and Dodec, the data are averages of two independent samples and the error value represents the difference in solubilization between the two samples.

measurement for the Dec and Dodec polymers was done to ensure it was not due to systematic error. The Dec polymer at 33% esterification showed the largest disparity between runs, but overall, the other polymers showed smaller differences. An explanation for this dip in SE from the Dec and Dodec polymer solutions would require more investigation, but it may be caused by intrinsic differences in the rhodopsin sample (e.g. membrane surface charge, fluidity, or protein/lipid ratio) or the stock polymer solution (e.g. hydrophobic blocks, or aggregation). Since the ROS disc membrane contains rhodopsin and lipids in a fixed ratio, the dip in SE is likely due to a variation in the Dec and Dodec polymer solutions, even though all functionalized SMAs were synthesized using the same feedstock. The differences in the polymer

solutions could be studied in more detail using small-angle x-ray scattering and transmission electron microscopy techniques.[2,3] The Bruce and Long groups are actively investigating how the preparation, purification, and storage of polymer solutions affect the protein extraction process.[4]

The first step in the proposed mechanism of SMALP formation involves the SMA copolymer binding to the surface of the membrane. The negative charge density of SMA is repulsed by the overall negative charge of the membrane surface.[5] Although the functionalized SMA copolymers have less negative charge overall, the hydrophobicity of the polymer appears to influence protein extraction as well. Between the alkoxy ethoxylate functionalized SMAs, the longer, more hydrophobic sidechains Dec and Dodec seem to extract less rhodopsin, particularly at high degrees of esterification. The But and DEG polymers both have six-atom sidechains, but DEG is more hydrophilic because of the ether units present. While DEG did not efficiently extract PSI from thylakoid membranes, it solubilized ~90% rhodopsin in ROS disc membranes at 15% and 44% esterification. The amount of rhodopsin solubilized decreases to 65% at 70% esterification. On the other hand, But at ~70% esterification solubilized nearly all of the rhodopsin in the sample. Overall, functionalized SMA copolymers efficiently extract rhodopsin from ROS disc membrane regardless of the sidechain length, percent esterification, or hydrophobicity of the polymer. DEG and TEG have previously displayed a tolerance to divalent cations, so their ability to efficiently extract protein from a phospholipid-rich environment enables various workup methods for many other proteins.

The second step in SMALP formation involves the insertion of the hydrophobic monomer unit into the lipid bilayer. From the results presented above, we wondered if the differences in hydrophobicity between the short versus long sidechain lengths of alkoxy ethoxylate functionalized SMAs was the reason for the differences in the solubilization of rhodopsin. We hypothesized that higher temperature, which causes the membrane to become more fluid, would allow the hydrophobic moieties to insert more readily and thus extract rhodopsin more efficiently. To test this idea, ROS membrane suspensions were warmed in a thermostatted water bath set to 30°C for 15 minutes. After the polymers were added, the samples were mixed well and then placed back in the water bath for an additional 15 minutes before centrifuging to remove the insoluble material.

Figure 4.1.3 shows how the percent SE as a function of percent esterification changes as temperature increased. We tested the two longest sidechains for the alkoxy ethoxylate functionalized SMAs, since the shorter sidechains already efficiently solubilize rhodopsin at room temperature. The Dec and Dodec polymers show a noticeable increase in percent SE as temperature increases, whereas the DEG and TEG polymers show very little difference. Therefore, polymers with long hydrophobic sidechains may require a higher degree of membrane fluidity to insert between the lipid tails and extract protein efficiently.

Static photobleaching measurements show that solubilization of rhodopsin by the functionalized SMAs results in loss of the functional integrity at 1.5% (w/v) copolymer, similar to unfunctionalized SMA at high concentration. Many samples

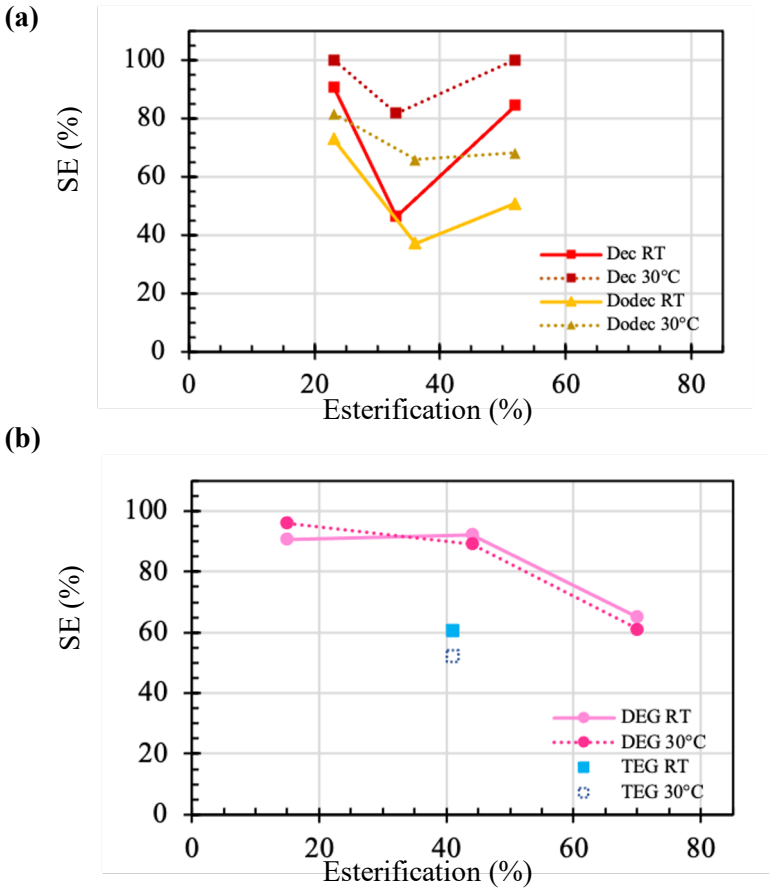

Figure 4.1.3 Percent solubilization efficiency (SE) as a function of percent esterification for **(a)** alkoxy ethoxylate and **(b)** ethylene glycol functionalized SMA copolymers at room temperature (RT) and 30°C.

contained $Meta_{460}$, which is a spectral form typically detected during the deactivation of rhodopsin. However, rhodopsin solubilized by TEG contained a final composition of about 65% $Meta_{380}$ and 35% $Meta_{480}$, which is similar to what is observed in the native membrane environment. We questioned if a hydrophilic variant of SMA would be less disruptive to rhodopsin's photoactivation kinetics because the hydrophobic moieties might interact with the cholesterol binding site on rhodopsin and prevent

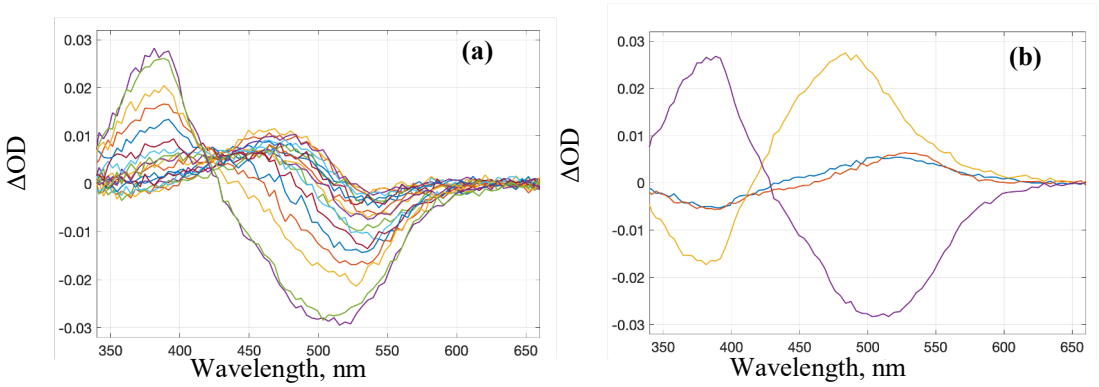

Figure 4.1.4 (a) Light-induced absorption difference spectra of rhodopsin solubilized by TEG recorded from 1 μs to 2 s. **(b)** The b-spectra corresponding to lifetimes 0.31 ms (blue line), 18 ms (red line), 0.23 s (yellow line), and the time-independent final spectrum (purple line) produced by global exponential fit to the time-dependent absorption spectra.

reaction progress. Therefore, we decided to investigate the kinetics of rhodopsin solubilized with TEG in more detail. Time-resolved optical absorption measurements from 1 μs to 2 s were performed at room temperature as detailed in Chapter 2.3. Figure 4.1.4a shows the difference spectra recorded for rhodopsin solubilized with TEG. Global exponential fit of the data matrix resulted in apparent lifetimes of 0.31 ms, 18 ms, and 0.23 s, and the b-spectra corresponding to these lifetimes are shown in Figure 4.1.4b. The lifetimes from the time-resolved experiment show that the reaction progress of rhodopsin solubilized by TEG is very slow, and hence the kinetic analysis of the sample was not pursued further.

4.2 Diisobutylene Maleic Acid Copolymer

Additional copolymers that incorporate maleic acid have been developed to

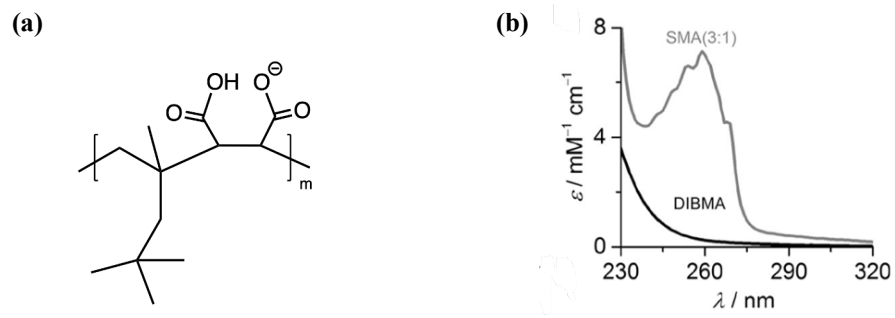

Figure 4.2.1 (a) Chemical structure of diisobutylene-maleic acid (DIBMA) copolymer at 50% ionization (on average, m ≈ 37 and M_n = 12 kDa). **(b)** Molar extinction coefficients (ε) of SMA(3:1) and DIBMA as functions of wavelength (λ). Figure from doi.org/10.1002/anie.201610778.

improve pH stability and sensitivity to divalent cations. Diisobutylene maleic acid (DIBMA) has recently gained popularity, especially with spectroscopists (Figure 4.2.1). The aliphatic diisobutylene group does not interfere in the far-UV range like the aromatic styrene group in SMA, which is useful for certain techniques, such as circular dichroism.[6,7] DIBMA is able to solubilize proteins directly from membrane suspensions, but it forms larger sized lipid particles (termed DIBMALPs). It also maintains the overall thickness of the membrane and has less of an impact on lipid chain order.[8]

The DIBMA copolymer appeared to be a good candidate to test our hypotheses for the slow rates observed in rhodopsin-SMALPs. We presumed that the larger particle size formed with DIBMA would be less restrictive and allow for the large conformational changes required for the protein to reach the active state. ROS were prepared as described in Chapter 2.1. The membrane pellet was resuspended in Tris buffer [10 mM tris(hydroxymethyl)aminomethane, 100 mM NaCl, pH 7.8 at room

temperature] to obtain a concentration of rhodopsin around 0.9-1.2 mg/mL (22-30 μM). DIBMA was purchased from Anatrace. An appropriate volume of 5% (w/v) DIBMA in Tris buffer was added to obtain the various molar ratios of DIBMA/rhodopsin. The samples were mixed well and then centrifuged at 17,000 x g for 20 minutes to isolate the solubilized material.

Similar to SMA, static photobleaching experiments showed that the amount of rhodopsin solubilized increased with increasing DIBMA concentrations (Figure 4.2.2a). In the samples prepared with a DIBMA/rhodopsin molar ratio of 25, roughly 25% of rhodopsin was solubilized, compared to 75% for the same ratio of SMA(3:1)/rhodopsin. Additionally, the amount of light scattering removed from the rhodopsin-DIBMALP samples to correct the spectra required a combination of λ^{-2} and λ^{-4} functions (Figure 4.2.2b). On the other hand, rhodopsin-SMALP samples only required a λ^{-4} function, and thus suggests that DIBMA formed larger particles. Both the lower yield of protein and larger particle size when using DIBMA compared to SMA

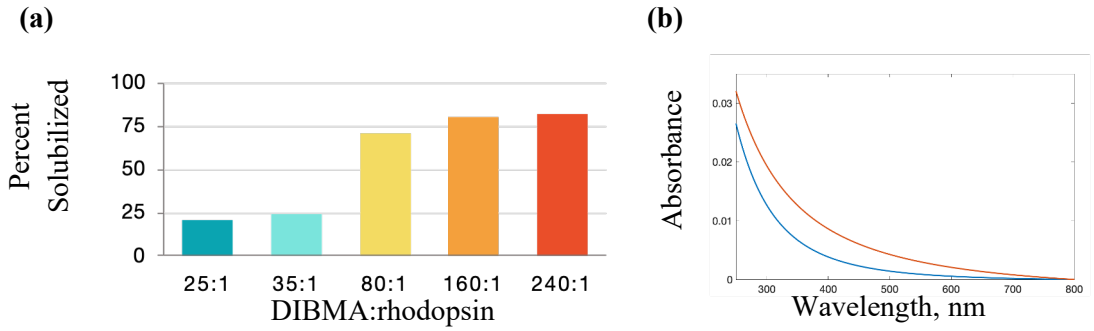

Figure 4.2.2 (a) Solubilization efficiency of DIBMA as a function of the ratio of DIBMA units per rhodopsin units. **(b)** Scattering functions required to correct spectra collected from static photobleaching experiments. For molar ratio of 25 polymer/rhodopsin, SMA(3:1) required λ^{-4}*0.08 (blue), and DIBMA required λ^{-4}*0.03+λ^{-2}*0.04 (red).

presented here are in agreement with findings published by A.J. Rothnie and co-workers.[8] Interestingly, rhodopsin did not appear to get "stuck" at a 480 nm photoproduct in samples prepared with a high molar ratio of DIBMA/rhodopsin, unlike SMA. Therefore, we decided to investigate the activation of rhodopsin in DIBMALPs in more detail. The time-resolved absorption difference spectra recorded from 1 μs to 5.6 s for the rhodopsin-DIBMALPs prepared at ratio 100 (rD100) are shown in Figure 4.2.3a. Global exponential fitting resulted in apparent lifetimes of 0.10 ms, 1.8 ms, 0.14 s, and 1.5 s with the b-spectra displayed in Figure 4.2.3b. The time-resolved absorption difference spectra recorded from 1 μs to 5.6 s for the rhodopsin-DIBMALPs prepared at ratio 500 (rD500) are shown in Figure 4.2.3c. Global exponential fitting resulted in apparent lifetimes of 14 ms and 1.4 s with the b-spectra displayed in Figure 4.2.3d.

The reaction progress of rhodopsin in DIBMALPs is similar to SMALPs. The b-spectra for the low ratio DIBMA sample, rD100, are similar to the low ratio SMA sample, rS10. The first b-spectrum shows the partial decay of the Lumi intermediate into the Meta I_{380} intermediate. The second lifetime, 1.8 ms, is 2.4 times longer than the second lifetime detected in the native membrane, and the corresponding b-spectrum has the shape of a Lumi minus $Meta_{480}$/$Meta_{380}$ difference spectrum. The DIBMA sample shows significantly more $Meta_{380}$ formed at this step. The third and fourth b-spectra both have the shape of a $Meta_{480}$ minus $Meta_{380}$ difference spectrum. The third b-spectrum has a higher amplitude than the fourth b-spectrum, which indicates that most of the Schiff base deprotonation does not occur in the slowest step. However, it is still approximately 20 times slower than the last step in the membrane.

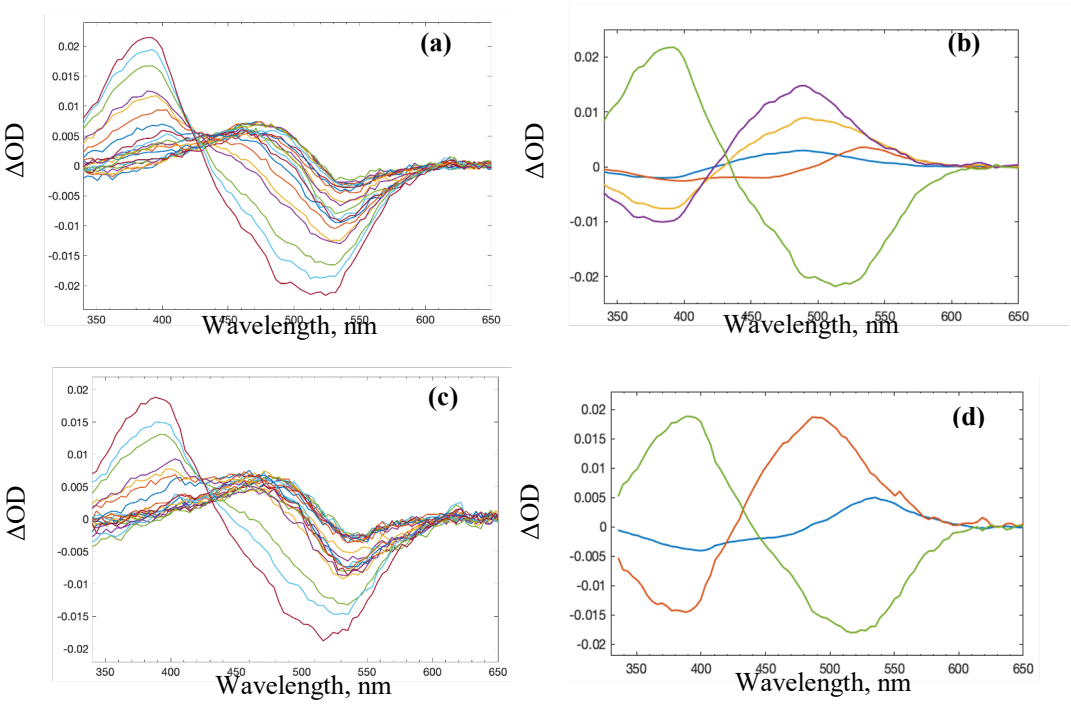

Figure 4.2.3 (a) Light-induced absorption difference spectra of rhodopsin in rD100, recorded from 1 µs to 5.6 s. **(b)** The b-spectra corresponding to 0.10 ms (bs_1, blue), 1.8 ms (bs_2, red), 0.14 s (bs_3, yellow), 1.5 s (bs_4, purple), and the time-independent final spectrum (bs_0, green), produced by global exponential fit to the time-dependent absorption spectra. **(c)** Light-induced absorption difference spectra of rhodopsin in rD500, recorded from 1 µs to 5.6 s. **(d)** The b-spectra corresponding to 14 ms (bs_1, blue), 1.4 s (bs_2, red), and the time-independent final spectrum (bs_0, green), produced by global exponential fit to the time-dependent absorption spectra.

For the rD500 sample, the faster b-spectrum (14 ms) looks like a Lumi minus $Meta_{480}$/$Meta_{380}$ spectral change, and only the slower b-spectrum (1.4 s) shows the conversion of protonated forms into unprotonated ones. Notably, the 460 nm absorbing form, which is known to be part of the deactivation process, does not appear with the 380 nm absorbing form at a high molar ratio of DIBMA/rhodopsin as it did with SMA. While the kinetics are slower, the absence of a 460 nm absorber suggests that

DIBMALPs may be less disruptive to the protein dynamics.

4.3 Lauryl Maltose Neopentyl Glycol Detergent

Novel amphipathic detergents have been designed to enable high resolution structural determination of membrane proteins.[13,14] Specifically, branched amphiphiles like lauryl maltose neopentyl glycol (LMNG) have been reported to solubilize a number of membrane proteins, and they display greater stability than detergents containing a single alkyl chain like DDM (Figure 4.3.1).[15–17] LMNG consists of two maltose units and two dodecyl chains linked to a central quaternary carbon. The central quaternary carbon restricts the mobility of the detergent molecules and enables a higher degree of packing, thus stabilizing proteins in such a way that promotes conformational homogeneity.[17]

LMNG is gaining popularity for structural studies of GPCRs. Thus, we tested how well rhodopsin retained its functional properties when solubilized by the detergent. ROS were prepared as described in Chapter 2.1. The membrane pellet was

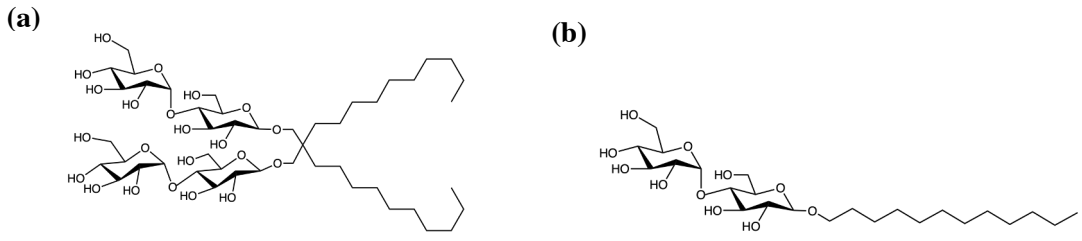

Figure 4.3.1 **(a)** Chemical structure of lauryl maltose neopentyl glycol (LMNG). CMC(H_2O) ~0.01 mM/0.001%. **(b)** Chemical structure of dodecyl-β-D-maltopyranoside (DDM). CMC(H_2O) ~0.17 mM/0.009%.

resuspended in Tris buffer [10 mM tris(hydroxymethyl)aminomethane, 100 mM NaCl, pH 7.8 at room temperature] to a final volume of 1 mL. The final concentration of rhodopsin was 0.9 mg/mL (23 μM). LMNG was purchased from ThermoFisher. A recent model of an activated rhodopsin-transducin complex found that ~70-80 LMNG detergent units surround rhodopsin in the micelle.[16] An appropriate volume of 5% (w/v) LMNG was added to the samples to reach a ratio of ~130 LMNG units/rhodopsin units, which is a little more than enough to form the micelle. The samples were placed on a nutator for 1 hour at 4°C, and then centrifuged at 27,000 x g for 5 minutes to isolate the LMNG-solubilized rhodopsin (rLMNG). The amount of solubilized rhodopsin in solution was 0.7 mg/mL (~17 μM).

Time-resolved optical absorption measurements from 1 μs to 200 ms were performed at room temperature as detailed in Chapter 2.3. Figure 4.3.2a shows the difference spectra recorded for rhodopsin in rLMNG. Global exponential fit of the data matrix resulted in apparent lifetimes of 25 μs, 0.29 ms, 2.8 ms, and 20 ms, and the b-spectra corresponding to these lifetimes are shown in Figure 4.3.2b. The b-spectra were converted into intermediate spectra for the straight sequential mechanism, and the intermediate spectra were decomposed into sums of the spectral forms as discussed in Chapter 2.5. The experimental absolute spectra (solid lines), along with the reproduced spectra to determine the composition (dashed lines), are displayed in Figure 4.3.2c. The time evolution of the Lumi, $Meta_{480}$, and $Meta_{380}$ spectral forms is compared in Figure 4.3.2d for rhodopsin in the membrane (solid lines) and rhodopsin in rLMNG (dashed lines).

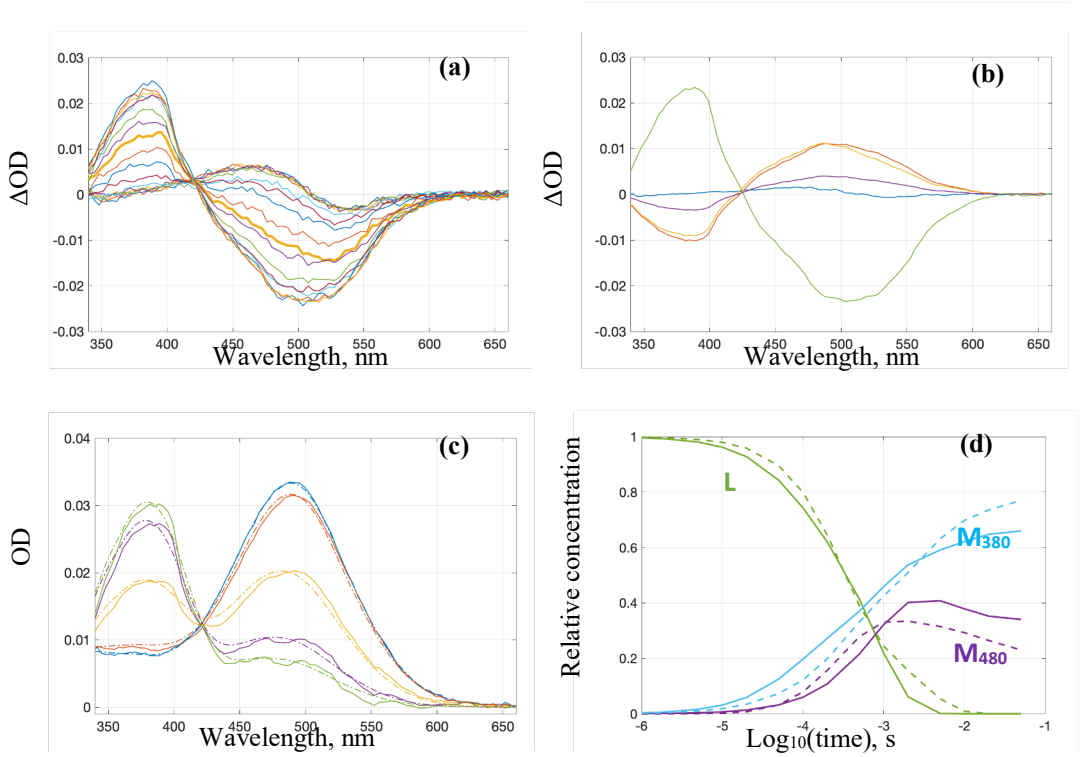

Figure 4.3.2 (a) Light-induced absorption difference spectra of LMNG-solubilized rhodopsin (rLMNG), recorded from 1 µs to 200 ms, with the spectrum at 1 ms displayed in bold. **(b)** The b-spectra corresponding to 25 µs (bs_1, blue), 0.29 ms (bs_2, red), 2.8 ms (bs_3, yellow), 20 ms (bs_4, purple), and the time-independent final spectrum (bs_0, green), produced by global exponential fit to the time-dependent absorption spectra. **(c)** Absolute spectra of the straight sequential intermediates calculated from the b-spectra (solid lines). The scheme was constructed based on the apparent lifetimes. Reproduction of the absolute spectra using the spectral forms to determine the composition matrix (dashed lines). **(d)** Time evolution of the Lumi (L), $Meta_{480}$ (M_{480}), $Meta_{380}$ (M_{380}) during the photoreaction in membrane (solid lines) and rLMNG (dashed lines).

When rhodopsin is solubilized with DDM, the photoreaction pathway favors the formation of Meta I_{380} over formation of Meta I_{480} in the double-square scheme. When rhodopsin is solubilized with a minimal amount of LMNG, a significant amount of the 480 nm absorber is formed to reach Meta II, which is what we observe in native

membrane suspensions. However, the amount of 480 nm absorber decreases if excess LMNG is used to solubilize rhodopsin. Despite incomplete solubilization occurring with low concentrations of LMNG, it is important to add the minimal amount required to form a micelle for studies of rhodopsin kinetics at ambient temperature. We tested whether removal of the excess LMNG could restore the rhodopsin photokinetics and whether the active-state composition seen in samples prepared at low LMNG/rhodopsin ratios could be reached. We carried out buffer exchange on the sample using a MWCO centrifugal filter (10kDa) and replaced the solution with a LMNG-free buffer. A comparison of the photoproducts before and after excess LMNG removal showed no spectral difference, thus the changes are not reversible. It is difficult to remove detergents with low critical micelle concentrations (CMC), so it takes longer to wash away excess LMNG if a high concentration is used to solubilize more protein.

4.4 Membrane Scaffold Proteins

Amphipathic helical protein belts, termed membrane scaffold proteins (MSPs), have been used as a suitable system for structural and functional studies of membrane proteins (Figure 4.4.1).[9–11] They allow membrane proteins to self-assemble into discoidal lipid bilayers, which are 8-16 nm in diameter depending on the length of the MSP and the stoichiometry of lipids used in the process. In most cases, the lipid molecules are synthetic, but lipid molecules extracted from biological membranes can be used as well. Rhodopsin encapsulated by MSP-nanodiscs that were prepared with the traditional assembly method have been reported to improve optical properties of

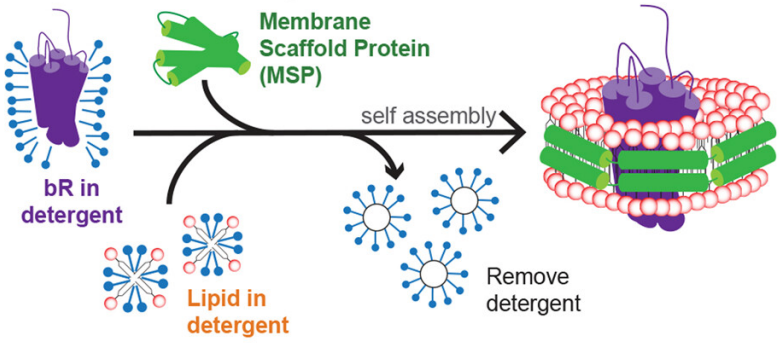

Figure 4.4.1 Schematic diagram showing traditional membrane scaffold protein (MSP) nanodisc assembly with membrane protein bacteriorhodopsin (bR) as an example. Figure from doi.org/10.1038/s41598-018-31925-1

samples without perturbing the activation sequence of rhodopsin.[12]

To investigate the photoactivation kinetics of rhodopsin using a more native approach to the assembly of MSP-nanodiscs, additional lipids were not added to the sample after rhodopsin was solubilized from ROS disc membranes. Rather, the lipids present in the sample after the detergent-solubilization step remained until the addition of MSP. ROS were prepared as described in Chapter 2.1. The membrane pellet was resuspended in 500 mL of 1% (w/v) dodecyl-β-D-maltopyranoside (DDM) in Tris buffer [10 mM tris(hydroxymethyl)aminomethane, 100 mM NaCl, pH 7.8 at room temperature]. The sample was mixed well and allowed to sit at room temperature for 15 minutes in the dark. Afterwards, the sample was centrifuged again at 17,000 x g for 20 minutes to isolate the solubilized material. The final concentration of rhodopsin was 1.2 mg/mL (~30 μM). MSP 1E3D1 was generously provided by the Farrens lab at Oregon Health and Science University. An appropriate volume of MSP 1E3D1 (100 μM) was added to the samples to achieve 2x molar equivalence, and then the samples

were placed on a nutator for 1 hour at 4°C. The rhodopsin MSP-nanodiscs (rMSP) were transferred to ½ volume of pre-washed Bio-Beads SM-2 and placed on the nutator for an additional hour. After detergent was removed, the nanodiscs were centrifuged at 17,000 x g for 5 minutes to sediment the Bio-Beads. The final concentration of rhodopsin in the MSP-nanodiscs was 0.6 mg/mL (~15 μM).

Time-resolved optical absorption measurements from 1 μs to 1 s were performed at room temperature as detailed in Chapter 2.3. Figure 4.4.2a shows the difference spectra recorded for rhodopsin in rMSP. Global exponential fit of the data matrix resulted in apparent lifetimes of 70 μs, 0.46 ms, 4.2 ms, and 0.11 s, and the b-spectra corresponding to these lifetimes are shown in Figure 4.4.2b. The b-spectra were converted into intermediate spectra, and the intermediate spectra were decomposed into sums of the spectral forms as discussed in Chapter 2.5. The experimental absolute spectra (solid lines), along with the reproduced spectra to determine the composition (dashed lines), are displayed in Figure 4.4.2c. The time evolution of the Lumi, $Meta_{480}$, and $Meta_{380}$ spectral forms in Figure 4.4.2d compare rhodopsin in the membrane (solid lines) and rhodopsin in rMSP (dashed lines).

Fitting the data for the rMSP sample required four apparent lifetimes to produce acceptable residuals with no spectral structures above the noise level, which demonstrates again that the classical sequential model is not a valid representation of rhodopsin kinetics at ambient temperature. The time course of the spectral forms for the rMSP sample shows a decay of the Lumi form into the $Meta_{480}$ and $Meta_{380}$ forms at early times, followed by an equilibration of the latter two forms on the millisecond

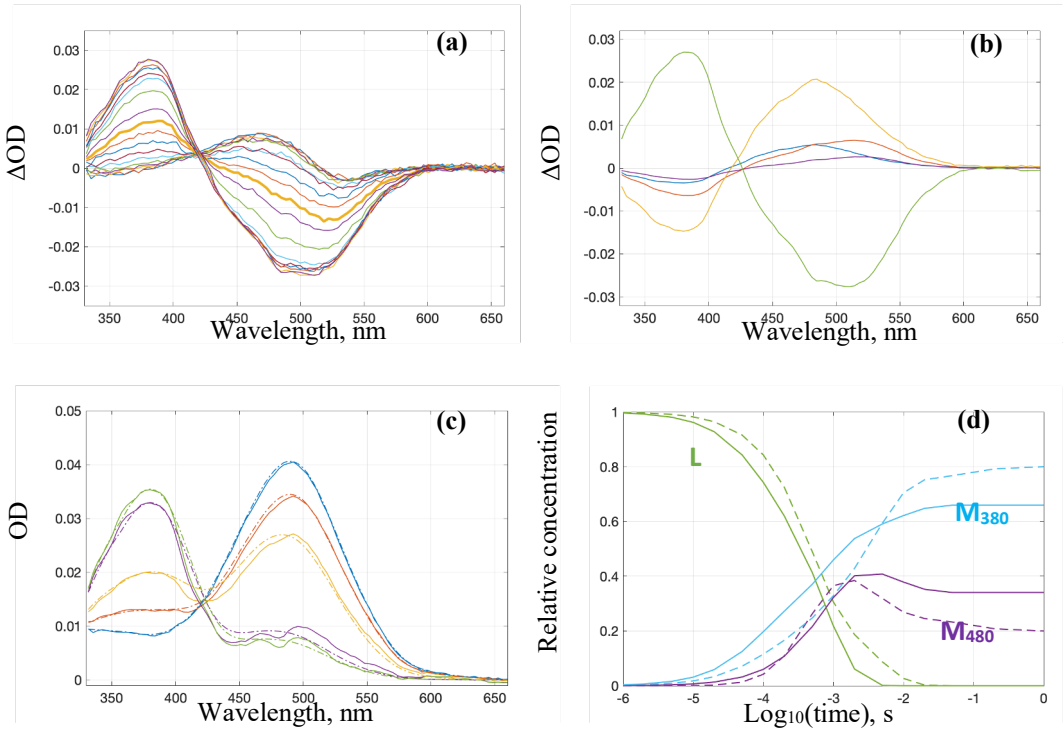

Figure 4.4.2 (a) Light-induced absorption difference spectra of rhodopsin in native lipid MSP-nanodiscs (rMSP), recorded from 1 µs to 1 s, with the spectrum at 1 ms displayed in bold. **(b)** The b-spectra corresponding to 70 µs (bs_1, blue), 0.46 ms (bs_2, red), 4.2 ms (bs_3, yellow), 0.11 s (bs_4, purple), and the time-independent final spectrum (bs_0, green), produced by global exponential fit to the time-dependent absorption spectra. **(c)** Absolute spectra of the straight sequential intermediates calculated from the b-spectra (solid lines). The scheme was constructed based on the apparent lifetimes. Reproduction of the absolute spectra using the spectral forms to determine the composition matrix (dashed lines). **(d)** Time evolution of the Lumi (L), $Meta_{480}$ (M_{480}), $Meta_{380}$ (M_{380}) during the photoreaction in the membrane (solid lines) and rMSP (dashed lines).

timescale. The last intermediate spectrum contains the $Meta_{480}$ and $Meta_{380}$ forms in a 1:4 ratio. Interestingly, the third b-spectrum shows the largest $Meta_{480}$-to-$Meta_{380}$ conversion occurs within tens of milliseconds, which is comparable to the last step in the membrane. The similarity between the kinetics of rhodopsin in the MSP-nanodisc

and the membrane sample, as well as the considerable amount recovered after detergent removal, suggests that MSP-nanodiscs may be the most appropriate for kinetic and dynamic studies of membrane proteins.

4.5 References

(1) Brady, N. G.; Workman, C. E.; Cawthon, B.; Bruce, B. D.; Long, B. K. Protein Extraction Efficiency and Selectivity of Esterified Styrene–Maleic Acid Copolymers in Thylakoid Membranes. *Biomacromolecules* 2021, *22* (6), 2544–2553. https://doi.org/10.1021/acs.biomac.1c00274.

(2) Su, G. M.; Cordova, I. A.; Brady, M. A.; Prendergast, D.; Wang, C. Combining Theory and Experiment for X-Ray Absorption Spectroscopy and Resonant X-Ray Scattering Characterization of Polymers. *Polymer* 2016, *99*, 782–796. https://doi.org/10.1016/j.polymer.2016.06.068.

(3) Craig, A. F.; Clark, E. E.; Sahu, I. D.; Zhang, R.; Frantz, N. D.; Al-Abdul-Wahid, M. S.; Dabney-Smith, C.; Konkolewicz, D.; Lorigan, G. A. Tuning the Size of Styrene-Maleic Acid Copolymer-Lipid Nanoparticles (SMALPs) Using RAFT Polymerization for Biophysical Studies. *Biochimica Et Biophysica Acta Bba - Biomembr* 2016, *1858* (11), 2931–2939. https://doi.org/10.1016/j.bbamem.2016.08.004.

(4) Workman, C. E.; Cawthon, B.; Brady, N. G.; Bruce, B. D.; Long, B. K. Effects of Esterified Styrene–Maleic Acid Copolymer Degradation on Integral Membrane Protein Extraction. *Biomacromolecules* 2022. https://doi.org/10.1021/acs.biomac.2c00928.

(5) Scheidelaar, S.; Koorengevel, M. C.; Pardo, J. D.; Meeldijk, J. D.; Breukink, E.; Killian, J. A. Molecular Model for the Solubilization of Membranes into Nanodisks by Styrene Maleic Acid Copolymers. *Biophys J* 2015, *108* (2), 279–290. https://doi.org/10.1016/j.bpj.2014.11.3464.

(6) Oluwole, A. O.; Danielczak, B.; Meister, A.; Babalola, J. O.; Vargas, C.; Keller, S. Solubilization of Membrane Proteins into Functional Lipid-Bilayer Nanodiscs Using a Diisobutylene/Maleic Acid Copolymer. *Angewandte Chemie Int Ed* 2017, *56* (7), 1919–1924. https://doi.org/10.1002/anie.201610778.

(7) Guo, R.; Sumner, J.; Qian, S. Structure of Diisobutylene Maleic Acid Copolymer (DIBMA) and Its Lipid Particle as a “Stealth” Membrane-Mimetic for Membrane

Protein Research. *Acs Appl Bio Mater* 2021, *4* (6), 4760–4768. https://doi.org/10.1021/acsabm.0c01626.

(8) Gulamhussein, A. A.; Uddin, R.; Tighe, B. J.; Poyner, D. R.; Rothnie, A. J. A Comparison of SMA (Styrene Maleic Acid) and DIBMA (Di-Isobutylene Maleic Acid) for Membrane Protein Purification. *Biochimica Et Biophysica Acta Bba - Biomembr* 2020, *1862* (7), 183281. https://doi.org/10.1016/j.bbamem.2020.183281.

(9) Bayburt, T. H.; Grinkova, Y. V.; Sligar, S. G. Self-Assembly of Discoidal Phospholipid Bilayer Nanoparticles with Membrane Scaffold Proteins. *Nano Lett* 2002, *2* (8), 853–856. https://doi.org/10.1021/nl025623k.

(10) Denisov, I. G.; Sligar, S. G. Nanodiscs for Structural and Functional Studies of Membrane Proteins. *Nat. Struct. Mol. Biol.* 2016, *23* (6), 481–486. https://doi.org/10.1038/nsmb.3195.

(11) Yeh, V.; Lee, T.-Y.; Chen, C.-W.; Kuo, P.-C.; Shiue, J.; Chu, L.-K.; Yu, T.-Y. Highly Efficient Transfer of 7TM Membrane Protein from Native Membrane to Covalently Circularized Nanodisc. *Sci Rep-uk* 2018, *8* (1), 13501. https://doi.org/10.1038/s41598-018-31925-1.

(12) Tsukamoto, H.; Szundi, I.; Lewis, J. W.; Farrens, D. L.; Kliger, D. S. Rhodopsin in Nanodiscs Has Native Membrane-like Photointermediates. *Biochemistry* 2011, *50* (22), 5086–5091. https://doi.org/10.1021/bi200391a.

(13) Sadaf, A.; Cho, K. H.; Byrne, B.; Chae, P. S. Chapter Four - Amphipathic Agents for Membrane Protein Study. *Methods Enzymol* 2015, *557*, 57–94. https://doi.org/10.1016/bs.mie.2014.12.021.

(14) Stetsenko, A.; Guskov, A. An Overview of the Top Ten Detergents Used for Membrane Protein Crystallization. *Crystals* 2017, *7* (7), 197. https://doi.org/10.3390/cryst7070197.

(15) Möller, I. R.; Merkle, P. S.; Calugareanu, D.; Comamala, G.; Schmidt, S. G.; Loland, C. J.; Rand, K. D. Probing the Conformational Impact of Detergents on the Integral Membrane Protein LeuT by Global HDX-MS. *J Proteomics* 2020, *225*, 103845. https://doi.org/10.1016/j.jprot.2020.103845.

(16) Gao, Y.; Westfield, G.; Erickson, J. W.; Cerione, R. A.; Skiniotis, G.; Ramachandran, S. Isolation and Structure–Function Characterization of a Signaling-Active Rhodopsin–G Protein Complex. *J Biol Chem* 2017, *292* (34), 14280–14289. https://doi.org/10.1074/jbc.m117.797100.

(17) Lee, S.; Ghosh, S.; Jana, S.; Robertson, N.; Tate, C. G.; Vaidehi, N. How Do Branched Detergents Stabilize GPCRs in Micelles? *Biochemistry-us* 2020, *59* (23), 2125–2134. https://doi.org/10.1021/acs.biochem.0c00183.

CHAPTER 5 Analyzing the Effects of Amphipathic Polymers on Rhodopsin

5.1 Polymer Groups Influence the Solubilization Efficiency

With rhodopsin, we were able to quantify the amount of protein removed from the hydrophobic environment of the lipid bilayer and solubilized in an aqueous solution with absorption spectroscopy. The presence of anionic lipids in the bilayer causes repulsion with negatively charged polymers and hinders the polymer from binding to the membrane surface.[1] DIBMA has a greater proportion of carboxylate groups than the commonly used SMA variants SMA(3:1) and SMA(2:1). The increase in negative charge was expected to decrease the yield of pure protein, which is what we observed with rhodopsin. DIBMA solubilized a smaller amount of rhodopsin than the SMAs at the same molar ratio of polymer:protein.

The addition of divalent cations may improve solubilization efficiencies with DIBMA. It has been reported that the association of Mg^{2+} and Ca^{2+} ions with DIBMA increases the protein extraction yields from *E. coli* membranes.[2] The neutralization of the negative charges allows the polymer to adhere to the surface of the membrane more readily. The addition of divalent cations was not tested with rhodopsin, but it could be useful if the aliphatic polymer is preferred for an experiment to avoid interference with UV absorption. Although an effective way to increase the amount of solubilized protein, these conditions are often not physiological and may not be ideal for studies intended to be as native-like as possible.

Alternatively, solubilizing biological membranes with glyco-DIBMA

copolymer may improve protein extraction yields.[3] Diisobutylene maleic anhydride reacts with meglumine, forming an amide bond and reducing the polymer's overall negative charge. This change increases the polymer's affinity for the membrane, most notably with anionic lipids, and increases the protein-extraction efficiency in near-physiological conditions. While the yield of the solubilized product would be higher, the hydrophobic monomer remains the same, and the reaction progress of rhodopsin is predicted to be slow.

5.1A Partial Esterification of SMA Copolymers

The series of SMA copolymers with varying extents of functionalization allowed us to investigate how the identity of the sidechains impacts protein solubilization. Alkoxy ethoxylate and ethylene glycol groups react with only a partial amount of the maleic acid monomers. The polymers were characterized to determine the extent of esterification, but the average molecular weights are unknown. Since we could not calculate approximate polymer:protein molar ratios, the results were compared separately from unfunctionalized SMA. All ROS disc membrane aliquots were mixed with functionalized SMA at a final concentration of 1.5% (w/v).

I hypothesized that the functionalized SMAs would increase the solubilization efficiency of rhodopsin since esterification of the maleic acid monomer decreases the overall negative charge of the polymers. The functionalized SMAs were very efficient at solubilizing rhodopsin, especially with short alkoxy ethoxylate sidechains. We observed a decrease in the amount of solubilized rhodopsin with long alkoxy ethoxylate sidechains or the presence of ethylene glycol units. Increasing the hydrophobicity of

the polymers has been reported to enhance the ability of the polymers to extract membrane proteins,[4] so I questioned why the longer alkoxy ethoxylate sidechains resulted in lower solubilization efficiencies.

One idea is that the polymer structure influences the amount of protein extracted, either from the styrene monomers being hidden or the polymer adopting a more coiled conformation. The second step in the formation of SMALPs is the insertion of the hydrophobic moiety into the core of the lipid bilayer, and unfunctionalized SMA is very efficient at extracting rhodopsin from the ROS disc membrane. The styrene moiety may be less exposed when surrounded by the long sidechains, thus it is less likely to insert into the lipid bilayer. It is interesting to note that the amount of rhodopsin solubilized with the short alkoxy ethoxylate sidechains was high regardless of the percent esterification.

In contrast, the amount of rhodopsin solubilized with long alkoxy ethoxylate sidechains decreased as the percent esterification increased. Therefore, the solubilization efficiency was impacted when the long sidechains were more frequent. This trend supports the idea that the presence of long aliphatic chains makes the styrene moiety more hidden in the polymer. Furthermore, the additional groups on the polymer may result in a coiled conformation as opposed to extended due to increasing polymer-polymer interactions. This change to the polymer structure would also result in the styrene moiety being less available to insert into the hydrophobic core and form lipid particles.

5.2 Polymer Groups Alter the Functional Properties

Amphipathic copolymers show great promise as alternative solubilizing agents and are becoming popular for structural studies of membrane proteins. Therefore, it is important to define how the polymer-stabilized lipid environment affects the functional properties of membrane proteins. Studying solubilized rhodopsin with time-resolved optical absorption spectroscopy and comparing the results to native membrane suspensions provided us with a unique opportunity to assess how copolymers affect the solubilized protein. Our initial studies with SMA(3:1) showed that the photokinetics of rhodopsin was significantly slower in the polymer-bound lipid nanoparticles. This result led us to hypothesize that there were changes in the physical properties of the lipid bilayer, such as membrane fluidity, or specific interactions with the receptor, such as interactions with the cholesterol binding site (Figure 5.2.1). We studied different maleic acid-derived copolymers to elucidate how the functional groups influenced the photokinetics of rhodopsin. Ultimately, we wanted to determine if there were conditions that retained optimal functional integrity.

5.2A Changes in Membrane Fluidity

Membrane fluidity is essential for the significant conformational changes required to activate rhodopsin. The transition from metarhodopsin I to metarhodopsin II involves a helical rearrangement that requires the partial free volume space provided by the polyunsaturated acyl chains of the surrounding lipid molecules. Interactions between the polymer and lipid alter the membrane fluidity, thus limiting its ability to

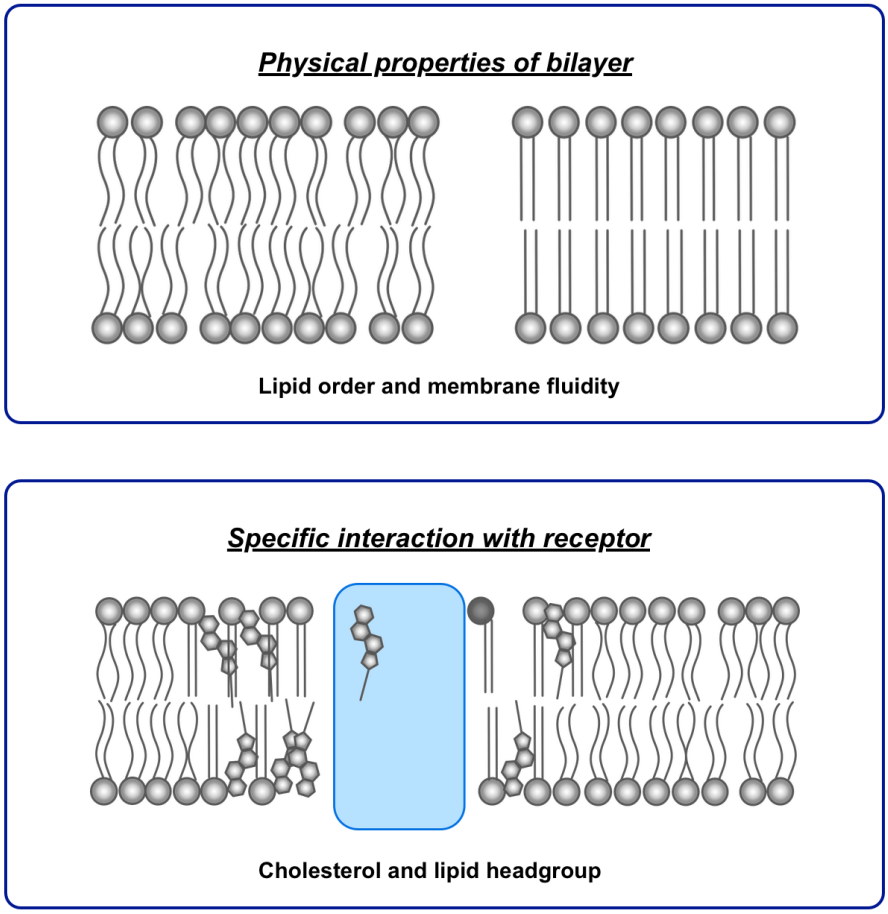

Figure 5.2.1 Ways the bilayer may influence GPCR function. Figure adapted from doi.org/10.1016/j.sbi.2011.09.007.

mimic the native environment. We examined how differences in lipid acyl chain perturbation and particle size may impact membrane fluidity.

The styrene moieties within SMA intercalate about midway along the acyl chains and interact with them directly.[5] SMA(3:1) perturbs the lipid acyl chain packing more than SMA(2:1), while DIBMA has the smallest effect.[6–8] Unlike the planar aromatic group, the bulky aliphatic group may be why DIBMA causes less perturbation

to the lipid packing than SMA. Perhaps perturbation causes the polymer to inhibit activation by disrupting the partial free volume or increasing lipid-protein interactions.[9] Therefore, I hypothesized that high styrene content would result in the least fluid lipid environment and cause rhodopsin to behave as it does at low temperature, while DIBMA would result in the most fluid lipid environment.

With SMA, the reaction progresses faster as the styrene:maleic acid ratio decreases, and only the rhodopsin-SMALPs prepared with low ratios of styrene:maleic acid showed an early formation of the $Meta_{380}$ spectral form. These results suggest that a decrease in perturbation by styrene causes the lipid environment to be more fluid and supports my hypothesis. However, the reaction progress of rhodopsin is even slower in DIBMALPs compared to the SMALPs. As DIBMA perturbs the lipid packing the least, I predicted a more fluid environment and this result did not support my hypothesis.

I also hypothesized that larger particle sizes increase membrane fluidity since there is more lipid in total. The light scattering present in spectra recorded during static photobleaching experiments showed that certain conditions resulted in larger particles. Various experiments, such as low versus high molar ratios of polymer:protein, SMALPs with and without lipid vesicles added, and DIBMA versus SMA, showed a difference in the particle size formed. Only one of the experiments, DIBMA versus SMA, yielded larger particle sizes but resulted in slower reaction progress. Rhodopsin-DIBMALPs and rhodopsin-SMALPs prepared at the same molar ratio of polymer:protein showed that rhodopsin surrounded by DIBMA exhibits slower

photokinetics at the late stages, which again contradicts my hypothesis about particle size and membrane fluidity.

Lipid acyl chain perturbation and the size of the lipid particle may certainly influence membrane fluidity. However, the experiments using DIBMA disproved each of my hypotheses regarding membrane fluidity that are outlined above, which led me to believe that an explanation for the slow reaction rates of rhodopsin was more complex than changes to the physical property of the bilayer.[10] It is important to note that there are other properties between lipid and protein that might be affected by the polymers, such as membrane curvature, lateral pressure, and bilayer thickness.

5.2B Interactions with the Cholesterol Binding Site

We also considered how specific interactions with the receptor influence GPCR function and how they may be affected by the polymers. Cholesterol comprises approximately 8-10 mol% of the total lipids of the ROS membrane and has been shown to modulate the coupling of the G-protein transducin to the active form of rhodopsin.[11,12] Excess cholesterol stabilizes rhodopsin and slows down the photokinetics due to the decrease in partial free volume required for the large conformational changes.[13] In GPCRs, cholesterol binding is mediated by a hydrophobic residue environment.[9] I hypothesized that the hydrophobic moieties of the polymers (styrene or diisobutylene) might interact with the proposed cholesterol binding site of rhodopsin in the inactive conformation and slow down the helical movement required to reach the active state.

After comparing the photoactivation of rhodopsin in different polymer-bound lipid particles, the reaction progress is faster as the styrene/maleic acid ratio decreases. This suggests that hydrophobic SMA variants may restrict the reaction progress due to weak intermolecular interactions with the proposed cholesterol binding site. The slow photokinetics of rhodopsin observed in DIBMALPs may be explained by this scenario as well. The aliphatic diisobutylene may have stronger interaction with the hydrophobic entrance that makes up the cholesterol binding site compared to the aromatic styrene group, which could be the reason why it takes longer for the reaction to progress in that system.

While these results support the hypothesis that hydrophobic polymers hinder the formation of the active state, we do not know if it is because the polymers are interacting with the cholesterol binding site. A few experiments could be done to answer this question. First, the introduction of cholesterol-lipid vesicles to the system is expected to slow the reaction progress even further if the cholesterol binding site is not occupied or blocked by the polymer. Next, a polymer with modifications to the hydrophobic monomer may be less impactful on the photokinetics of rhodopsin. The alkoxy ethoxylate- and ethylene glycol-functionalized SMAs present a new group added to the hydrophilic monomer, but unfortunately, they did not appear to improve the integrity of the membrane environment surrounding rhodopsin at high concentrations. Instead, polymers with different groups on the hydrophobic monomer, such as certain poly(acrylic acid) polymers,[4] may prevent interaction with the cholesterol binding site upon insertion into the lipid bilayer.

5.3 Conclusions and Future Direction

Altogether, we confirmed that amphipathic copolymers significantly affect the photokinetics of rhodopsin, especially when present in excess. While low polymer concentrations result in incomplete solubilization, it is critical to retain native membrane-like conditions. High concentrations of SMA disrupt the pathway, and the active state is not reached, thus rendering the solubilized protein not suitable for kinetic studies. Hydrophobic variations of SMA at low concentration favor the rhodopsin pathway through $Meta_{480}$. These effects may be due to the membrane fluidity of the lipid particle. SMA(3:1) copolymer is known to perturb lipid packing the most. We showed that adding lipid vesicles to samples with low SMA(3:1)/rhodopsin molar ratio formed larger particles that no longer showed a preference for the pathway through $Meta_{480}$. The earlier formation of unprotonated inactive forms (Meta I_{380}), which is observed at high temperatures, implies a less rigid membrane environment.

DIBMA is less disruptive to the activation sequence of rhodopsin than SMA, but the solubilization yield is lower, and the reaction progress is slower. DIBMA forms larger lipid particles and has been reported to be less impactful on lipid packing order, two conditions that are predicted to increase membrane fluidity. Consequently, the slower reaction progress hints that a specific polymer-protein interaction might affect the conformational changes required to reach the active state. It is unclear if the polymers interact with the cholesterol binding site in the inactive conformation, but excess cholesterol is also known to slow down the photoactivation of rhodopsin. As mentioned above, an experiment with cholesterol-lipid vesicles may provide

information about the state of the binding site.

We demonstrated that minimal concentrations of polymer might be suitable for kinetic membrane protein studies, and optimal conditions must be established first. In terms of retaining functional integrity, the nature of the polymer used is as important as the size of the lipid nanoparticle it produces. Amphipathic copolymers offer a huge advantage of avoiding the application of harmful detergents, but this work suggests that MSP-based nanodiscs may be more appropriate for studies involving rhodopsin photokinetics. The particle size and lipid composition are tunable, and the scaffold protein does not slow down the formation of late rhodopsin intermediates.

Now that we have established the ideal conditions to study rhodopsin photokinetics, we plan to study recombinantly expressed rhodopsin that contain single-point mutations that are involved in a genetic retinal disorder, retinitis pigmentosa. Some mutations result in opsin that is properly folded and transported to the correct cellular compartment, binds 11-*cis*-retinal, but eventually leads to degeneration due to their unstable nature.[14,15] Therefore, we have a unique opportunity to use spectroscopic tools to understand how rhodopsin may misfunction in this class of mutations associated to retinitis pigmentosa.

5.4 References

(1) Dörr, J. M.; Scheidelaar, S.; Koorengevel, M. C.; Dominguez, J. J.; Schäfer, M.; Walree, C. A. van; Killian, J. A. The Styrene–Maleic Acid Copolymer: A Versatile Tool in Membrane Research. *Eur. Biophys. J.* 2016, *45* (1), 3–21. https://doi.org/10.1007/s00249-015-1093-y.

(2) Danielczak, B.; Meister, A.; Keller, S. Influence of Mg2+ and Ca2+ on Nanodisc Formation by Diisobutylene/Maleic Acid (DIBMA) Copolymer. *Chem Phys Lipids* 2019, *221*, 30–38. https://doi.org/10.1016/j.chemphyslip.2019.03.004.

(3) Danielczak, B.; Rasche, M.; Lenz, J.; Patallo, E. P.; Weyrauch, S.; Mahler, F.; Agbadaola, M. T.; Meister, A.; Babalola, J. O.; Vargas, C.; Kolar, C.; Keller, S. A Bioinspired Glycopolymer for Capturing Membrane Proteins in Native-like Lipid-Bilayer Nanodiscs. *Nanoscale* 2021, *14* (5), 1855–1867. https://doi.org/10.1039/d1nr03811g.

(4) Marconnet, A.; Michon, B.; Prost, B.; Solgadi, A.; Bon, C. L.; Giusti, F.; Tribet, C.; Zoonens, M. Influence of Hydrophobic Groups Attached to Amphipathic Polymers on the Solubilization of Membrane Proteins along with Their Lipids. *Anal Chem* 2022, *94* (41), 14151–14158. https://doi.org/10.1021/acs.analchem.2c01746.

(5) Jamshad, M.; Grimard, V.; Idini, I.; Knowles, T. J.; Dowle, M. R.; Schofield, N.; Sridhar, P.; Lin, Y.; Finka, R.; Wheatley, M.; Thomas, O. R. T.; Palmer, R. E.; Overduin, M.; Govaerts, C.; Ruysschaert, J.-M.; Edler, K. J.; Dafforn, T. R. Structural Analysis of a Nanoparticle Containing a Lipid Bilayer Used for Detergent-Free Extraction of Membrane Proteins. *Nano Res* 2014, *8* (3), 774–789. https://doi.org/10.1007/s12274-014-0560-6.

(6) Grethen, A.; Oluwole, A. O.; Danielczak, B.; Vargas, C.; Keller, S. Thermodynamics of Nanodisc Formation Mediated by Styrene/Maleic Acid (2:1) Copolymer. *Sci Rep-uk* 2017, *7* (1), 11517. https://doi.org/10.1038/s41598-017-11616-z.

(7) Oluwole, A. O.; Danielczak, B.; Meister, A.; Babalola, J. O.; Vargas, C.; Keller, S. Solubilization of Membrane Proteins into Functional Lipid-Bilayer Nanodiscs Using a Diisobutylene/Maleic Acid Copolymer. *Angewandte Chemie Int Ed* 2017, *56* (7), 1919–1924. https://doi.org/10.1002/anie.201610778.

(8) Gulamhussein, A. A.; Uddin, R.; Tighe, B. J.; Poyner, D. R.; Rothnie, A. J. A Comparison of SMA (Styrene Maleic Acid) and DIBMA (Di-Isobutylene Maleic Acid) for Membrane Protein Purification. *Biochimica Et Biophysica Acta Bba - Biomembr* 2020, *1862* (7), 183281. https://doi.org/10.1016/j.bbamem.2020.183281.

(9) Sejdiu, B. I.; Tieleman, D. P. Lipid-Protein Interactions Are a Unique Property and Defining Feature of G Protein-Coupled Receptors. *Biophys. J.* 2020, *118* (8), 1887–1900. https://doi.org/10.1016/j.bpj.2020.03.008.

(10) Grime, R. L.; Logan, R. T.; Nestorow, S. A.; Sridhar, P.; Edwards, P. C.; Tate, C. G.; Klumperman, B.; Dafforn, T. R.; Poyner, D. R.; Reeves, P. J.; Wheatley, M. Differences in SMA-like Polymer Architecture Dictate the Conformational Changes

Exhibited by the Membrane Protein Rhodopsin Encapsulated in Lipid Nano-Particles. *Nanoscale* 2021, *13* (31), 13519–13528. https://doi.org/10.1039/d1nr02419a.

(11) Niu, S.-L.; Mitchell, D. C.; Litman, B. J. Optimization of Receptor-G Protein Coupling by Bilayer Lipid Composition II FORMATION OF METARHODOPSIN II-TRANSDUCIN COMPLEX*. *J Biol Chem* 2001, *276* (46), 42807–42811. https://doi.org/10.1074/jbc.m105778200.

(12) Jastrzebska, B.; Debinski, A.; Filipek, S.; Palczewski, K. Role of Membrane Integrity on G Protein-Coupled Receptors: Rhodopsin Stability and Function. *Prog. Lipid Res.* 2011, *50* (3), 267–277. https://doi.org/10.1016/j.plipres.2011.03.002.

(13) Albert, A. D.; Boesze-Battaglia, K. The Role of Cholesterol in Rod Outer Segment Membranes. *Prog Lipid Res* 2005, *44* (2–3), 99–124. https://doi.org/10.1016/j.plipres.2005.02.001.

(14) Tsukamoto, H.; Farrens, D. L. A Constitutively Activating Mutation Alters the Dynamics and Energetics of a Key Conformational Change in a Ligand-Free G Protein-Coupled Receptor. *J Biological Chem* 2013, *288* (39), 28207–28216. https://doi.org/10.1074/jbc.m113.472464.

(15) Xie, G.; D'Antona, A. M.; Edwards, P. C.; Fransen, M.; Standfuss, J.; Schertler, G. F. X.; Oprian, D. D. Preparation of an Activated Rhodopsin/Transducin Complex Using a Constitutively Active Mutant of Rhodopsin. *Biochemistry-us* 2011, *50* (47), 10399–10407. https://doi.org/10.1021/bi201126r.